Miner Petrol (2011) 102:135–161
DOI 10.1007/s00710-011-0169-3

SPECIAL ISSUE ACCESSORY MINERALS

Zircon from historic eruptions in Iceland: reconstructing storage and evolution of silicic magmas

Tamara L. Carley · Calvin F. Miller · Joseph L. Wooden · Ilya N. Bindeman · Andrew P. Barth

Received: 26 November 2010 / Accepted: 2 August 2011 / Published online: 26 August 2011

Abstract Zoning patterns, U-Th disequilibria ages, and elemental compositions of zircon from eruptions of Askja (1875 AD), Hekla (1158 AD), Öræfajökull (1362 AD) and Torfajökull (1477 AD, 871 AD, 3100 BP, 7500 BP) provide insights into the complex, extended, histories of silicic magmatic systems in Iceland. Zircon compositions, which are correlated with proximity to the main axial rift, are distinct from those of mid-ocean ridge environments and fall at the low-Hf edge of the range of continental zircon. Morphology, zoning patterns, compositions, and U-Th ages all indicate growth and storage in subvolcanic silicic mushes or recently solidified rock at temperatures above the solidus but lower than that of the erupting magma. The eruptive products were likely ascending magmas that entrained a zircon "cargo" that formed thousands to tens of thousands of years prior to the eruptions.

Editorial handling: I. Broska and D. Harlov

Electronic supplementary material The online version of this article (doi:10.1007/s00710-011-0169-3) contains supplementary material, which is available to authorized users.

T. L. Carley (✉) · C. F. Miller
Department of Earth & Environmental Sciences,
Vanderbilt University,
PMB 351805, 2301 Vanderbilt Place,
Nashville, TN 37235-1805, USA
e-mail: tamara.l.carley@vanderbilt.edu

J. L. Wooden
Stanford-USGS Micro Analysis Center, SHRIMP Lab,
Stanford University,
Green Earth Sciences Building, 367 Panama Street Room 89,
Stanford, CA, USA

I. N. Bindeman
Department of Geological Sciences,
University of Oregon,
1272 University of Oregon,
Eugene, OR 97403, USA

A. P. Barth
Department of Earth Sciences,
Indiana University-Purdue University, Indianapolis,
723 West Michigan Street, SL118,
Indianapolis, IN 46202, USA

Introduction

Icelandic volcanism is controlled by a hotspot in conjunction with a propagating mid-ocean ridge. Approximately 10–12% of rocks in Iceland are silicic (Walker 1966; Saemundsson 1979; Gunnarsson et al. 1998), which is unusually abundant in an intraoceanic setting (Jonasson 2007). Many workers have investigated silicic rocks in Iceland and debated petrogenetic explanations for their occurrence (e.g. Carmichael 1964; Macdonald et al. 1987; Gunnarsson et al. 1998; Jonasson 2007; Lacasse et al. 2003; Sverrisdottir 2007; Martin and Sigmarsson 2007, 2010). In this study, we describe the first use of zircon as a tool for investigating the pre-eruptive evolution of silicic magma in Iceland.

Zircon can provide critical insights into complex, extended histories of evolution, storage, and remobilization within magmatic systems. Uranium-lead and U-Th disequilibrium dating has demonstrated that volcanic zircons record several hundred k.y. of pre-eruption history in many but not all studied cases (e.g. Long Valley, USA, Reid et al. 1997; Taupo Zone, New Zealand, Brown and Fletcher 1999; Charlier et al. 2003, 2005; Mount St. Helens, USA, Claiborne et al. 2010a; Yellowstone, USA, Vazquez and Reid 2002; Bindeman et al. 2008; Crater Lake, USA, Bacon and Lowenstern 2005; Soufriere, Lesser Antilles, Schmitt et al. 2010; but in contrast to the Bishop Tuff, Crowley et al. 2007, Simon et al. 2008).

Disparate interpretations of this phenomenon have arisen: prolonged crystallization during the storage of

uneruptible magma (e.g. Reid et al. 1997; Brown and Fletcher 1999; Vazquez and Reid 2002) vs. inheritance of young zircon from rapidly remelted solid rock (e.g. Bindeman et al. 2001, 2008). Furthermore, zoning patterns and elemental compositions are sensitive indicators of conditions of zircon growth and further document the complexity of histories of magma storage zones (e.g. Pupin 2000; Watson and Harrison 2005; Claiborne et al. 2006).

Uranium-thorium dating is limited to young events (<~350 ka), but precision down to a few k.y. is attainable by in situ secondary ion mass spectrometry (SIMS) methods (Bacon and Lowenstern 2005; Claiborne et al. 2010a). Combining precise in situ U-Th dating with elemental analyses of zircon grains reveals records of thermal and compositional evolution of melts and provides insights into timing and rates of magma-system processes (Claiborne et al. 2010a).

We have examined zircon from silicic volcanic rocks from recent (primarily historical) eruptions in a variety of tectonic regions of Iceland that are characterized by distinct thermal structures and potential magma generating conditions: Askja 1875 AD, on-rift; Torfajökull 871 and 1477 AD, on-rift, but near a rift termination; Hekla 1158 AD, transitional; and Öræfajökull 1362 AD, off-rift (see Fig. 1 for general locations and Table 1 for precise locations and sample descriptions). We also analyzed zircon from two prehistoric on-rift eruptions of silicic lava (~7500 BP, ~3100 BP) at Torfajökull.

By sampling young eruptions we are able to confidently establish very precise ages (± <1 yr for the historic eruptions) for the eruptions, which can readily be compared to measured U-Th disequilibrium ages, representing timing of zircon growth. Furthermore, the absolute uncertainty in U-Th age decreases with decreasing age, so it is expected that zircon grains in younger eruptions can be dated more precisely than zircon from older eruptions. The prehistoric eruptions that we study from Torfajökull are both less than 10 ka, much younger than the upper limit of effective U-Th dating.

Overview of investigated volcanoes

We provide below a summary of current knowledge of these four well-studied volcanic systems based on published descriptions as well as on our own observations and sampling. Extensive previous work at each volcanic center permits us to focus on the contributions of zircon to understanding of silicic magmatism in Iceland.

Askja

Askja is an "on rift" volcano, located near the southern end of the actively-spreading Northern Volcanic Zone (NVZ), one of the major components of the axial rift zone that cuts across Iceland (Sparks et al. 1981; Thordarson and Larsen 2007). The base of the central volcano comprises a ring-like structure of sub-glacial palagonite (hydrated and devitrified basalt; Sparks et al. 1981) with the 3–4 km diameter Öskjuvatn caldera from the 1875 eruption, itself nested inside of an older, 8 km diameter caldera from a pre-historic eruption (Sparks et al. 1981). Since the 1875 eruption it has been recognized that the Askja central volcano is linked with the Sveinagja fissures located 70 km to the north, with contemporaneous eruptions of rhyolite from the caldera and basalt from the fissures (Sparks et al. 1981; Thordarson and Larsen 2007). Ejecta from Askja are chemically distinguished from other volcanic deposits in Iceland with comparable SiO_2 contents by their relatively high whole-

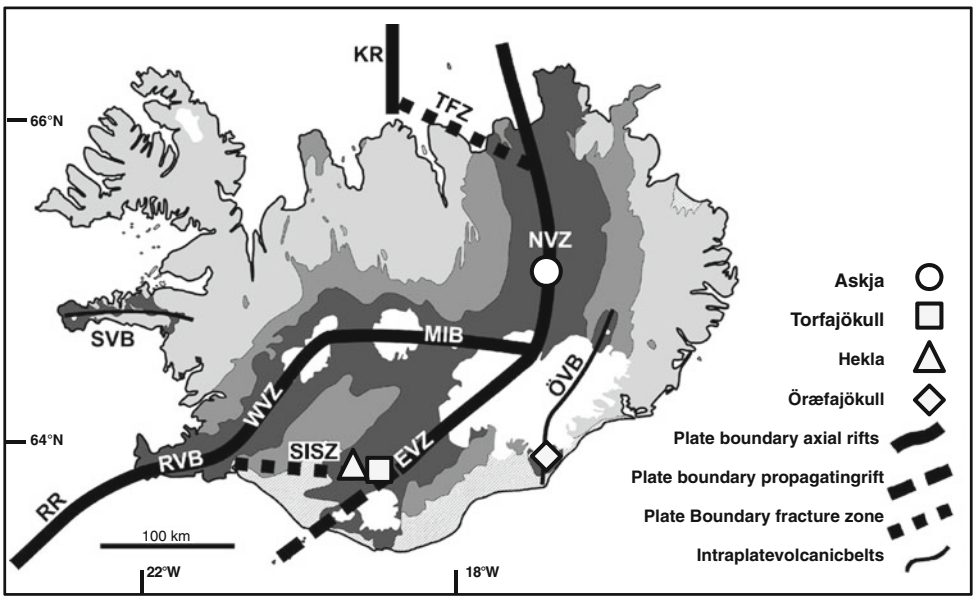

Fig. 1 General locations of volcanoes examined in this study: Askja, Öræfajökull, Hekla and Torfajökull. Major tectonovolcanic features as given by Thordarson and Hoskuldsson (2002): RVB, Reykjanes Volcanic Belt; WVZ, EVZ, NVZ: Northern, Eastern and Western Volcanic Zones; OVB, Oraefi Volcanic Belt; SVB, Snaefellsness Volcanic Belt; MIB, Mid-Icelandic Belt; RR, Reykjanes Ridge; TFZ, Tjornes Fracture Zone; KR, Kolbeinsey Ridge; SISZ: South Iceland Seismic Zone; WF, Westfjords. Figure modified from Thordarson and Hoskuldsson (2002)

Table 1 Overview of eruptions and samples discussed in this study

Volcano	eruption date	erupted vol. (km^3)	sample location	sample coordinates[a]	sample type	SiO_2 (mass %)[b]	Zr (ppm)	zircon sat. temp (°C)[c]	initial $^{230}Th/^{232}Th$	$\delta^{18}O/^{16}O$ (‰)
Askja	1875 AD (IC48)[d]	2[e]	Top of ridge to the NE of Lake Öskjuvatn	28 W	Pumice	69.0	301	814	1.01[f]	Low
				041996						0.08 (plagioclase)
				7214591						−0.24 (plagioclase)
										−1.14 (clinopyroxene)
										−2.67 (magnetite)
										−2.27 (magnetite)
Öræfajökull	1362 AD (IOHn1)	10[e]	Small pit on SSE side of HWY 1, between Hofnes Farm and Hnappavellir turn-off	28 V	Pumice	72.4	813	932	0.99[g]	Normal
				0420478						5.17 (plagioclase)
				7086216						3.76 (clinopyroxene)
Hekla	1158 AD (IHB1)	0.33[e]	S. end of the Burfell located W. of Hekla, 2 m from ravine-top.	27 W	Pumice	68.7	718	920	0.97[h]	Normal
				0558938						5.08 (plagioclase)
				7106903						4.14 (clinopyroxene)
Torfajökull	1477 AD (ITN1)	0.01[i]	Lava flowing into Lake Frostastadavatn, at water line	27 W	Lava	66.3	668	890	0.9[j]	Low
				0595113						3.96 (whole rock)
				7099846						4.02 (whole rock)
	871 AD (ITHn)	0.16	Flow access near Laufafell, near (but before) 2nd river ford when approaching from S.	27 V	Lava	66.9	605	880	0.9	3.8 (whole rock)[k]
				0584358						
				7093649						
	3100 BP (3A03)	0.4	Dómadalshraun vent	Unavailable[l]	Lava	70.1	755	920	0.9	Unavailable
	7500 BP (5A03)	0.01	Dómadalshraun vent	Unavailable	Lava	71.9	778	925	0.9	Unavailable

[a] All coordinates are given in UTM Hjorsey (1955)

[b] Whole-rock geochemistry values for major elements are normalized to 100%

[c] Calculated using whole rock geochemistry and the methods of Watson and Harrison 1983

[d] Sample name given in parentheses beneath eruption date

[e] Larsen et al.(1999)

[f] Value from Condomines et al. (1981), measured using Askja 1875 AD dacite

[g] Value from Rose-Koga and Sigmarsson 2008

[h] Value from Sigmarsson, written communication, 2009

[i] All Torfajökull lava volumes taken from Macdonald et al (1990)

[j] Value from Zellmer et al. (2004, 2008)

[k] Value from Gunnarrsson et al. (1998)

[l] Zircons from the 3100 and 7500 BP eruptions of Torfajökull were from the Brown et al. (2004) study; precise sampling locations unavailable.

rock MgO and TiO_2 (Larsen et al. 1999) and most depleted $\delta^{18}O$ values (Muehlenbachs et al. 1974; Table 1). There have been only two occurrences of silicic magma erupting from the Askja caldera since the last deglaciation, first at the start of the Holocene (Sigvaldason 2002) and most recently the 1875 AD eruption examined in this study. Tholeiitic ferrobasalt and icelandite were erupted in 1875, as well as silicic and mixed pumices that have a compositional range of 58–74 wt% SiO_2 (Macdonald et al. 1987).

Some argue that extreme fractional crystallization alone can explain the origin of rhyolites from ferrobasalt (e.g. Wood 1978; Wood et al. 1979) while others cite fractional crystallization as the dominant process at work, with contributions from minor wall-rock assimilation, partial melting of silicic xenoliths, and basaltic injection explaining complex trace element geochemistry and low $\delta^{18}O$ values (Sigurdsson and Sparks 1981; Macdonald et al. 1987).

The 1875 AD eruption that formed the Öskjuvatn caldera produced 2 km^3 of silicic tephra (Sigurdsson and Sparks 1981; Macdonald et al. 1987; Larsen et al. 1999; Jonasson 2007). Some of the pumice ejected during the 1875 eruption was purely rhyolite ("white rhyolite" of Sparks et al. 1981), and this rhyolite is the host of the zircon for our study. There are also many pumice clasts with streaks of tholeiitic basalt, ferrobasalt and icelandite that are thought to represent magma mingling immediately before, or during, eruption (Macdonald et al. 1987).

Öræfajökull

Öræfajökull is located in the ÖræfiVolcanic Belt (ÖVB), an active intraplate volcanic zone located at the southern margin of the Eastern Volcanic Flank Zone (Prestvik et al. 2001; Thordarson and Larsen 2007; Selbekk and Tronnes 2007). The ÖVB is thought to be a potential "embryonic" (Thordarson and Larsen 2007), or incipient, rift, but for our purposes in this study we classify Öræfajökull as "off-rift" because of its distance (~50 km east) from the dominant axial rift zone (Prestvik et al. 2001; Thordarson and Hoskuldsson 2002; Thordarson and Larsen 2007; Selbekk and Tronnes 2007). The central volcano, the largest in Iceland, is thought to sit unconformably on uplifted and eroded Tertiary basalt (Larsen et al. 1999; Prestvik et al. 2001; Selbekk and Tronnes 2007). The base of the volcano is composed dominantly of subglacially erupted pillow basalt and hyaloclastite breccia and tuff (Prestvik et al. 2001; Selbekk and Tronnes 2007). Explosive post-glacial eruptions at Öræfajökull are thought to have originated from an ice-filled summit caldera with an area of ~14 km^2 (Selbekk and Tronnes 2007; Sharma et al. 2008). The volcanic deposits from Öræfajökull are compositionally bimodal (basalt and rhyolite) with notably high Na_2O and low MgO concentrations that distinguish it from rift-zone volcanoes (Larsen et al. 1999; Prestvik et al. 2001). It has been proposed that rhyolite at off-rift volcanoes like Öræfajökull is likely produced by fractional crystallization because new, hot, magma is injected into crust that is "thicker, cooler and stronger" (Selbekk and Tronnes 2007) than crust in an extensional zone and better able to dissipate heat without reaching solidus temperatures (Martin and Sigmarsson 2007, 2010). Normal $\delta^{18}O$ values (Table 1) are consistent with derivation of Öræfajökull silicic rocks by fractional crystallization.

There have been two explosive eruptions at Öræfajökull in historical times, first in 1362 AD and again in 1727 AD (Larsen et al. 1999; Selbekk and Tronnes 2007). The 1362 AD Plinian eruption that we have examined produced ~10 km^3 of silicic tephra, and is thought to have been "the most voluminous explosive silicic eruption" (Larsen et al. 1999) in Iceland in historical times (Thorarinsson 1958; Sharma et al. 2008). The compositional homogeneity of phenocrysts and matrix glasses throughout the entire recognized 1362 AD deposit is unique (Selbekk and Tronnes 2007). This striking homogeneity is taken to indicate a uniform and extremely well-equilibrated magma chamber, or upper zone in an atypically large silicic magma chamber (Selbekk and Tronnes 2007).

Hekla

Hekla is located at the western end of a propagating rift that extends southwestward from the Eastern Volcanic Zone (EVZ; Sverrisdottir 2007), and its tectonic setting is therefore considered "transitional." The volcanic center forms a NE-SW trending ridge built upon basaltic hyaloclastite of Pleistocene age (Sverrisdottir 2007). Silicic magma erupts from a 5 km-long summit fissure and from short radial fissures on the flanks of the volcano, while basalt erupts from the Vatnafjöll fissure swarm that runs parallel to the Hekla ridge (Gronvold et al. 1983; Thordarson and Larsen 2007; Sverrisdottir 2007). Hekla erupts lava and tephra that span compositions from basalt through icelandite to rhyolite (Sverrisdottir 2007). Approximately 95% of the intermediate lava that has been erupted in Iceland in historical times has been erupted from Hekla (Thordarson and Larsen 2007). The 1158 AD silicic tephra that we sampled is distinguished from other historical silicic tephras based on its relatively high FeO and CaO, and low K_2O contents (Larsen et al. 1999; Table 2).

It has been observed that the SiO_2 content of magma ejected from Hekla decreases throughout the course of a single eruption. The SiO_2 content of the first erupted material correlates with the period of time that has passed

Table 2 Major and trace element geochemistry of pumice and lava samples

	Askja 1875 AD	Öræfajökull 1362 AD	Hekla 1158 AD	Torfajökull 871 AD	1477 AD	3100 BP	7500 BP
Major elements (mass%)							
SiO_2	71.9	72.4	68.7	66.9	66.3	70.1	71.9
Al_2O_3	12.6	13.2	14.6	14.4	14.9	14.9	14.1
$Fe_2O_{3\ (T)}$	4.63	3.97	5.95	4.97	5.79	3.26	2.70
MnO	0.11	0.10	0.15	0.10	0.12	0.08	0.07
MgO	0.86	0.04	0.30	1.85	0.96	0.22	0.13
CaO	2.79	1.10	2.78	2.43	2.51	1.06	0.75
Na_2O	3.78	5.40	4.69	4.75	5.20	5.54	5.52
K_2O	2.28	3.40	2.37	3.86	3.60	4.47	4.52
TiO_2	0.89	0.27	0.40	0.69	0.54	0.32	0.24
P_2O_5	0.20	0.02	0.07	0.10	0.08	0.04	0.02
(LOI)	1.23	1.97	1.03	0.24	0.17	0.41	0.50
Selected trace elements (ppm)							
Rb	52	71	48	94	81	112	114
Sr	107	64	219	115	140	81	51
Ba	372	669	578	418	483	505	421
Cs	0.3	0.6	0.4	0.8	0.6		
Pb	<5	<5	<5	7	<5		
Nb	40	94	91.9	127	114	135	160
Ta	2.28	4.74	4.47	6.3	6.34		
Co	4.5	1.4	2.1	10.7	6		
Cr	<0.5	7.1	9.8	72	8.4		
Ni	2	2	5	45	8		
V	27	<5	<5	54	39		
Zr	388	813	718	605	668	755	778
Hf	10.7	21.1	18.2	16.2	17.7		
Th	7.46	10.3	9.81	15.2	14.1		
U	2.19	3.07	2.92	4.58	4.3		
Sc	11.6	1.43	9.84	6.12	6.88		
Y	57	102	76	56	59	76	96
La	40.1	69.5	70.1	78	74.8	94	94
Ce	81.2	150	143	152	154		
Pr	9.67	18.3	17.3	16.7	17.3		
Nd	39	73.9	68.2	60.3	61.9		
Sm	9.14	17.2	15.1	11.9	12.3		
Eu	2.13	3.06	3.65	1.72	2.3		
Gd	9.63	18	14.6	11.1	11.5		
Tb	1.66	3.23	2.48	1.77	1.92		
Dy	10.3	19.4	14.6	10.8	11.5		
Ho	2.15	3.82	2.86	2.12	2.23		
Er	6.45	11.1	8.27	5.98	6.48		
Tm	0.98	1.67	1.25	0.88	0.96		
Yb	6.5	11.3	8.48	5.91	6.3		
Lu	1.06	1.81	1.34	0.91	1		

Major element compositions are normalized to 100% (excluding LOI).

since the last eruption, with higher SiO_2 compositions following longer periods of repose (e.g. Gronvold et al. 1983; Sverrisdottir 2007; Oswald et al. 2007). Historical eruptions at Hekla, including the 1158 AD eruption, have followed a generally consistent pattern, starting with a brief (<1 hr) but vigorous subplinian to Plinian event in which a great deal of magma is evacuated from the chamber, followed by a period of simultaneous lava fountaining and tephra ejection, and concluding with intermittent Strombolian eruptions (e.g. Gronvold et al. 1983; Thordarson and Larsen 2007).

Partial melting of tholeiitic crust with subsequent magma mixing has been proposed as a mechanism for silicic magma generation at Hekla, based on Th isotopes and major-mineral composition and zoning (Sverrisdottir 2007). Fractional crystallization of a persistent basaltic andesite magma chamber beneath the volcano has also been suggested as a viable process for creating silicic magma, based on mineral assemblages and compositions, as well as whole-rock and glass compositions that display continuous (i.e. no gaps) yet inflected (i.e. non-linear) trends for some elements (e.g. Zr) extending from mafic to silicic end members (Oswald et al. 2007). These inflected trends are inconsistent with a history of magma mixing, and are thus viewed as support of fractional crystallization. Normal $\delta^{18}O$ values (Table 1) are consistent with rhyolite genesis by fractional crystallization of an initial 4.8‰ basalt.

Torfajökull

Torfajökull is located in a volcanically active belt at the intersection of the Eastern Volcanic Zone (EVZ) and the South Iceland Seismic Zone (SISZ), and thus it is situated in a "propagating rift" setting (Gunnarsson et al. 1998). The Torfajökull central volcano is a large caldera structure, 30 km long in the WNW-ESE direction and 18 km wide in the NE-SW direction, built upon 10 Ma tholeiitic crust (Gunnarsson et al. 1998). More than 80% of the volcano exposed at the surface is composed of silicic extrusive rocks, and with a volume of ~225 km^3 and an area of ~450 km^2, Torfajökull is the largest exposure of silicic rock in all of Iceland, and perhaps in the entire oceanic crust (Gunnarsson et al. 1998; Larsen et al. 1999). Torfajökull is the largest high-temperature geothermal region in Iceland, which has led to pervasive hydrothermal alteration of crust in the area (Arnorsson et al. 1987; Gunnarsson et al. 1998). Postglacial rhyolite and basalt have erupted from linear fissures in the western part of the caldera, which is thought to be the most actively fissuring section of the ERZ (Gunnarsson et al. 1998). Basaltic volcanism often occurs at the nearby Veidivötn fissure swarm contemporaneously with rhyolitic eruptions from the Torfajökull caldera fissures (Blake 1984; Mork 1984; Jonasson 2007; Zellmer et al. 2008).

One explanation for silicic magmatism at Torfajökull is that >90% fractional crystallization of parental basalt has yielded sub-alkaline rhyolites, and continued fractionation of these sub-alkaline melts led to peralkaline rhyolite generation (Macdonald et al. 1990). This interpretation was based upon analysis of whole rock geochemical trends. An alternative interpretation is that magma influx related to rifting and fissuring of the crust in the Torfajökull area supplies heat necessary for partial melting of the hydrothermally altered crust (Gunnarsson et al. 1998). In this view, based upon whole-rock trace element geochemistry and low $\delta^{18}O$ values, the anatectic, silicic partial melt is stored and continues to evolve to its final composition by crystal fractionation before being erupted (Martin and Sigmarsson 2007; Zellmer et al. 2008).

In this study we examined four post-glacial (two pre-historic, two historic) eruptions of silicic lava: 7500 BP at Dómadalshraun (0.74 km^2, 0.0126 km^3), 3100 BP from the Dómadalshraun vent (1.13 km^2, 0.0396 km^3), 871 AD Hrafntinnuhraun flow (4.87 km^2, 0.160 km^3) and the 1477 AD Námshraun flow (0.87 km^2, 0.0084 km^3;Macdonald et al. 1990). They all represent variably-low $\delta^{18}O$ magmas (3–4‰, Table 1, Gunnarsson et al. 1998; Martin and Sigmarsson 2007), requiring assimilation of variable amounts of low $\delta^{18}O$ crust for different eruptions.

Methods

Whole rock geochemistry

Samples of silicic pumice and lava were sent to Activation Laboratories (ActLabs, Ancaster, Ontario Canada) for lithogeochemical analyses, where they were initially pulverized in a steel mill. Actlabs applied a combination of inductively coupled plasma optical emission spectrometry (ICP), instrumental neuron activation analysis (INAA), inductively coupled plasma mass spectrometry (ICP-MS) and X-ray fluorescence spectrometry (XRF) to measure major and trace element concentrations (package code: 4E-Research+ICP/MS). Results, which were verified using a suite of internationally-recognized standards, can be found in Table 2.

Zircon separation methods

We removed individual zircon grains from bulk-rock samples by a process that included crushing, density separation by water table and heavy liquid (LST), magnetic

susceptibility separation by Frantz magnetic separator, and hand-picking. Approximately 5 kg of each sample was processed for mineral extraction. The Askja sample collected specifically for this study yielded no zircon by these methods. Zircon, separated by HF dissolution at the University of Oregon, from pumice previously collected from the same eruptive unit, was therefore used for our zircon analyses.

Zircon image analysis

Zircon grains were mounted in epoxy and polished to expose grain interiors. Once mounted, grains were imaged under a reflected light microscope and by cathodoluminescence (CL) on the JEOL JSM 5600 scanning electron microscope (SEM) at the Microanalysis Center shared by the US Geological Survey (USGS) and Stanford University (see On-line Appendix A for all CL images). We used reflected light and CL images to characterize zircon populations using the following criteria: maximum length, representative width, presence of discrete (typically CL-dark) centers, presence and character of zoning, and signs of resorption. We determined average characteristics for individual zircon populations from each sample in this study, and then conducted an inter-eruption comparison with the goal of identifying (a) universal morphological characteristics of historical zircon crystals from Icelandic volcanoes, and (b) unique morphological characteristics based on the individual volcanic system and setting.

Oxygen isotope analyses

Oxygen isotope analyses relied on duplicated analysis of 1–2 mg quantity of glass or mineral material and were performed by laser fluorination in the University of Oregon lab using MAT 253 gas source mass spectrometer (see Bindeman, 2008 for details).

Zircon SHRIMP-RG trace element analysis

The Stanford-USGS sensitive high resolution ion microprobe-reverse geometry (SHRIMP-RG) was used to determine Hf, U, Th, Ti and rare earth elements (REE) compositions of zircon. The basic operating parameters of the SHRIMP-RG, elemental suite analyzed, and data reduction techniques are as described in Claiborne et al. (2006, 2010b). A beam size of 15 μm was used in analysis, and spot placement was guided by CL and reflected light images. Where possible, multiple spots were placed on grains to discern compositional differences between grain interiors and rims. SHRIMP-Lab zircon standards MAD and VP10 were used to calibrate trace element analyses.

Zircon saturation temperatures and Ti-in-zircon thermometry

Zircon saturation temperatures were estimated using the equation:

$$\ln D_{Zr}^{zircon/melt} = (-3.8 - [0.85(M-1)] + 12900/T$$

where $D_{Zr}^{zircon/melt}$ is the concentration ratio of Zr in zircon to Zr in the host melt, Zr in zircon is taken to be ~476,000 ppm, M is the cation ratio (Na+K+2*Ca)/(Al*Si) of the melt, and T is temperature in Kelvin (Watson and Harrison 1983; Miller et al. 2003). For melt compositions, we used whole-rock geochemical analysis. Because our pumice and lava samples are dominantly unaltered volcanic glass with small volumes of phenocrysts (<10%), bulk analyses provide good estimates of melt composition at the time of eruption.

We estimated zircon crystallization temperatures using the Ti-in-zircon thermometer calibrated by Ferry and Watson (2007):

$$\log(\text{ppm Ti}-\text{in}-\text{zircon}) = (5.711\pm0.072) - (4800\pm86)/T(K) - \log a_{SiO2} + \log a_{TiO2}).$$

Temperatures calculated by this method are dependent on estimates of melt a_{TiO2} and a_{SiO2}. The a_{TiO2} in a typical silicic magma usually falls between 0.6 and 0.9 (Watson et al. 2006; Ferry and Watson 2007). Overestimating a_{TiO2} leads to an underestimate of temperature; for example, a calculation with an activity of 0.9 may yield a temperature of 777°C while an activity of 0.7 for the same sample will yield a temperature of 803°C. The estimated a_{TiO2} for melts with the compositions of our samples range from 0.4 to >1 (based on the method of Hayden and Watson (2007) and Ti concentrations in the whole-rock necessary to saturate rutile at 750–900°C; in all cases, calculated values approach or exceed unity at T=800°C). For consistency, we assumed a uniform a_{TiO2} of 0.7 (broadly consistent with our findings) to calculate Ti-in-zircon temperatures. The a_{SiO2} of quartz-undersaturated silicic melts is rarely less than 0.5 (Watson et al. 2006; Ferry and Watson, 2007; Hayden et al. 2007; cf. Carmichael et al. 1974), but overestimating a_{SiO2} can lead to temperatures that are too high by tens of degrees (°C); for example, a calculation with an activity of 1.0 may yield a temperature of 805°C while an activity of 0.7 for the same sample will yield a temperature of 782°C. Despite these potential errors, we chose to use an assumed a_{SiO2} of 1.0 in our calculations since zircon crystals are likely to grow in conditions near quartz saturation. Because we cannot quantify the degree to which our estimated activities stray from reality, we cautiously use the Ti-in-zircon thermometer to qualitatively examine intra- and inter-population thermal

relationships, rather than to place undue confidence in precise temperatures.

U-Th disequilibrium dating

Model ages determined by the U-Th disequilibrium method are well suited for determining precise (in an absolute sense) ages of growth of young (<350 ka) zircon, especially if initial $^{230}Th/^{232}Th$ of the melt is reasonably well known. Uranium-thorium disequilibrium ages were calculated using the method previously described by Lowenstern et al. (2000) and Charlier et al. (2005). Our decision to focus our efforts on historical eruptions allows us accurately identify a "zero" age at the time of eruption. Initial whole-rock $^{230}Th/^{232}Th$ ratios for individual volcanoes and, where available, individual eruptions, were taken from published literature (Table 1), and U-Th analyses of individual zircon grains were conducted using the SHRIMP-RG with a beam diameter of 30 μm, guided, as for elemental analyses, by CL images. SHRIMP-Lab zircon standards MAD, VP10 and R33 were used to verify the validity of our ages and define the U-Th equiline.

Results

Whole rock geochemistry and mineral assemblages

The Askja 1875 AD pumice sample is extremely crystal-poor (<1%), with minor plagioclase, clinopyroxene, Ti-Fe oxides and very sparse accessory zircon. Our geochemical analyses (Table 2) and physical observations of the coarse, low-density pumice are consistent with those published for "layer D" by Sparks et al. (1981) and Macdonald et al. (1987). The Öræfajökull 1362 AD pumice is also extremely crystal poor (<1%) with minor plagioclase, olivine, clinopyroxene, Fe-Ti oxides and accessory zircon (our observations; Selbekk and Tronnes, 2007). Our whole-rock results are typical of published results describing the erupted material (Table 2; Selbekk and Tronnes 2007; Sharma et al. 2008). Pumice from the 1158 AD eruption of Hekla is crystal-poor (<5%), with a phenocryst assemblage of plagioclase, fayalitic olivine, clinopyroxene, Fe-Ti oxides, apatite, and zircon. Whole rock geochemistry of our sample matches almost perfectly that of published compositions for 1158 AD tephra (cf. Larsen et al. 1999). The lavas that we collected from Torfajökull had <10% phenocrysts with mineral assemblages that include plagioclase, anorthoclase, clinopyroxene, Fe-Ti oxides, hornblende, olivine, apatite and zircon (our observations; Gunnarsson et al. 1998). Our whole-rock geochemical analyses for the prehistoric eruptions (3100 BP, 7500 BP) are consistent with published results, while historical (1477 AD, 871 AD) eruptions show compositions with lower SiO_2 and K_2O and higher Al_2O_3 and TiO_2 than published results (among other differences; Table 2; Macdonald et al. 1990).

Zircon morphology and zoning

Zircon populations (summarized in Table 3) are very sparse (<10/kg) and characteristically small (<150 μm average) in our samples. Internal and external morphology of zircon crystals (Fig. 2) is, for the most part, relatively simple and broadly similar from grain to grain and sample to sample. Euhedral shapes and thick euhedral internal zones with relatively subdued CL contrast are typical; most grains lack well-defined cores and oscillatory zoning is generally barely visible. Well-defined dark centers are relatively common only in Öræfajökull and historic Torfajökull zircon grains, sparser in prehistoric Torfajökull samples, and absent in zircon from Hekla and Askja. The dark centers of Öræfajökull zircon crystals are distinctly mottled, and sector zoning is observed only in zircon from the Öræfajökull sample. Rounded external morphology and internal zone boundaries are uncommon except for the historic Torfajökull samples (871 AD, 1477 AD), in which a majority of zircon grains display rounding.

U-Th Ages

Zircon from six dated samples (Table 4) display model age spectra spanning several tens of k.y., but each age spectrum is distinct in detail (continuous vs. discontinuous, skewed towards older or younger; Fig. 3a,b). Öræfajökull (1362 AD) zircon grew over a semi-continuous time span from approximately 35 ka to near-eruption (~0 ka). Hekla (1158 AD) zircon grew in a period spanning >40 ky. The calculated ages appear to define discrete clusters, but many more grains must be analyzed to fully assess the reality of episodic growth. Torfajökull 871 AD model ages are confined to 10–30 ka; the other Torfajökull samples display a broader, more scattered span of ages that preceded eruption by ~0–50 ka. Taken as a whole, the entire Torfajökull data set reveals apparently continuous zircon growth from near zero to 50 ka, with a well-defined maximum at 10 ka. Attempts to date Askja 1875 AD zircon were unsuccessful due to large errors related to very low U concentrations and Th-U ratios.

Minor and trace element geochemistry (U, Th, Hf, Ti, REE)

Uranium and Th concentrations in zircon have been widely studied because of the value of zircon U-Th-Pb geochronology, and Th/U ratios have been shown to correlate with zircon growth environments and with tectonic and lithospheric realms (Sawka and Chappell 1988; Bea 1996;

Table 3 Averaged observations of zircon population morphological features

Eruption	Count	Max length (μm)	Max. width (μm)	Aspect ratio[a]	Discrete interior[b,c]	Obvious zoning	Obvious rounding[d]
Askja 1875 AD (all)[e]	10	119	59	2	0.1	0.7	0.1
Askja 1875 AD (intact)	4	120	54	2.1	0.3	0.5	0.3
Öræf. 1362 AD (all)	39	133	38	2.5	0.5	0.8	0.2
Öræf. 1362 AD (intact)	20	131	40	3.3	0.6	1.0	0.2
Hekla 1158 AD (all)	46	166	43	3.3	0.2	0.7	0.1
Hekla 1158 AD (intact)	16	161	42	3.3	0.2	0.8	0.2
Torfa. 871 AD (all)	9	91	42	2	0.3	0.9	0.6
Torfa. 871 AD (intact)	5	108	41	2.5	0.6	0.8	0.6
Torfa. 1477 AD (all)	17	103	54	2	0.2	0.4	0.5
Torfa. 1477 AD (intact)	6	115	58	2	0.2	0.7	0.7
Torfa. 7500 BP (all)	37	112	64	1.7	0.2	0.7	0
Torfa. 7500 BP (intact)	16	128	63	2	0.4	0.8	0
Torfa. 3100 BP (all)	32	84	47	1.7	0.1	0.8	0
Torfa. 3100 BP (intact)	6	107	48	2	0.2	1.0	0
ALL SAMPLES (all)	191	123	49	2	2	0.7	0.2
ALL SAMPLES (intact)	72	132	48	2.5	2.5	0.8	0.2

[a] Aspect ratio (length/width) was determined for individual grains; the average is the mean of calculated aspect ratios.

[b] Data in columns titled "discrete center," "obvious zoning," and "obvious rounding" refers to the fraction of grains that display these features.

[c] A discrete center is identified as a dark interior that is distinguishable, with clear boundaries, from the rest of the surrounding zircon grain.

[d] Evidence of rounding (possible resorption) at grain rims and at the boundaries of discrete interiors.

[e] "all" refers to all recognizable zircon—both intact grains and fragments of grains.

O'Hara et al. 2001; Hoskin and Schaltegger 2003; Grimes et al. 2007). Hafnium is an indicator of fractionation, with higher concentrations suggesting growth from more evolved melts from which zircon has already been removed (e.g. Claiborne et al. 2006, 2010b). Titanium concentration has been shown to correlate with temperature of crystallization (Watson and Harrison 2005; Watson et al. 2006; Ferry and Watson 2007; Claiborne et al. 2010a,b). Rare

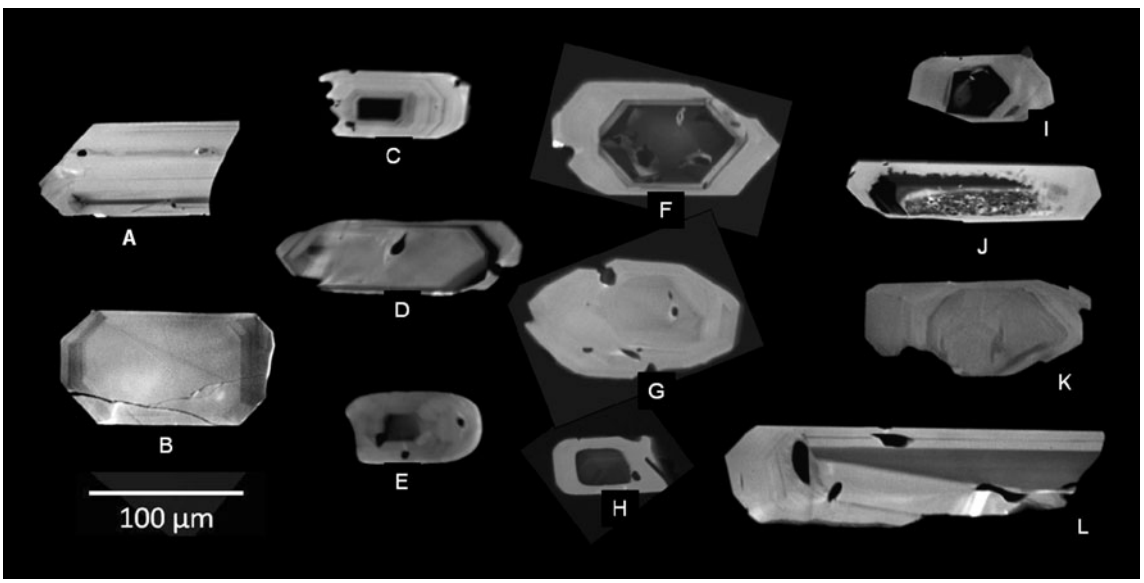

Fig. 2 Cathodoluminescence images of representative zircon crystals from this study. A-B: Askja; C-E: Torfajökull 871 AD; F-H: Torfajökull 1477 AD; I-J: Öræfajökull; K-L: Hekla. Grain B from Askja and C from Torfajökull display oscillatory zoning. Grains C, E, F and H from Torfajökull, I and J from Öræfajökull all have discrete dark centers. Grains E and H from Torfajökull have rounded centers and external form that are suggestive of resorption. Grain G from Torfajökull and K from Hekla have internal zoning features suggestive of resporption. Grain J from Öræfajökull has a dark, discrete, mottled interior zone

Table 4 In situ U-Th disequilibrium dating

zircon grain[a]	$^{238}U/^{232}Th$	$\pm^{238}U/^{232}Th$	$^{230}Th/^{232}Th$	$\pm^{230}Th/^{232}Th$	model age (years)	model error (+ years)	model error (− years)
Hekla (0.97)[b]							
1.1I-B	5.65	0.17	1.68	0.12	17786	4345	4178
1.3I-B	4.78	0.15	2.22	0.13	43230	7669	7164
10.1I-B	8.06	0.25	0.18	0.01	−11449	1421	1402
12.2C	2.93	0.09	1.36	0.06	24075	8175	7603
12.2C-B	4.45	0.14	1.76	0.12	28002	6659	6275
13.1I-B	3.85	0.12	1.15	0.08	7082	5094	4866
16.1I-B	4.80	0.15	1.56	0.10	18181	4820	4615
22.1I-B	4.52	0.14	1.06	0.07	2683	3885	3751
Oraefajokull (0.99)							
3.1T-B	2.66	0.08	1.09	0.06	6943	8169	7598
4.1C	2.46	0.08	1.12	0.04	10476	8572	7945
7.1T	2.50	0.08	1.40	0.07	34253	12238	10999
7.2C	2.53	0.08	0.95	0.03	−2570	6832	6428
7.2C-B	2.96	0.09	1.08	0.04	5124	6449	6088
8.1I	3.44	0.11	1.07	0.06	3563	4992	4773
9.1E-B	4.09	0.12	1.47	0.08	18426	5649	5370
15.3C	3.24	0.10	1.09	0.05	5017	5241	5000
15.3C-B	2.68	0.08	1.08	0.04	5695	7472	6991
16.1I	2.29	0.07	1.14	0.05	13058	10111	9250
20.1C-B	1.17	0.04	1.00	0.02	5290	101182	51494
Torfajokull (0.9) 1477 AD							
1.1I-B	5.49	0.17	1.28	0.09	9281	3271	3175
3.1I-B	2.61	0.08	1.49	0.07	45639	12331	11074
5.2C-B	2.82	0.09	1.10	0.03	12284	6202	5867
8.2I-B	3.73	0.11	1.42	0.07	22264	5672	5391
9.1C-B	4.84	0.15	1.29	0.06	11294	3370	3269
10.1I-B	4.38	0.13	1.25	0.07	11484	4057	3911
13.1C-B	2.84	0.09	1.10	0.04	12025	6279	5937
14.21-B	4.61	0.14	1.01	0.06	3372	3326	3228
871 AD							
1.1U	3.77	0.11	1.42	0.07	21862	5469	5207
4.1U	2.10	0.06	1.10	0.02	20332	10809	9831
5.1U	4.10	0.12	1.36	0.07	16920	4658	4466
2.1U	2.95	0.09	1.37	0.05	28198	7771	7253
3.1U	4.95	0.15	1.78	0.09	26521	4675	4482
3.2U	4.07	0.12	1.22	0.06	11431	4246	4087
6.1U	2.85	0.09	1.19	0.05	17715	7069	6638
7.1U	4.25	0.13	1.64	0.08	26926	5329	5080
8.1U	3.14	0.09	1.38	0.06	26263	7023	6597
9-1.1U	3.65	0.11	1.37	0.06	20472	5318	5070
9-4.1U	4.50	0.13	1.37	0.07	15182	4101	3952
3100 BP							
1	3.98	0.12	1.31	0.07	15550	4945	4730
2	2.94	0.09	1.49	0.07	37119	9376	8631
3.1	3.00	0.09	1.19	0.06	16219	6873	6464
4	3.66	0.11	1.10	0.06	8354	4838	4632
5	2.92	0.09	1.51	0.07	38649	9661	8872
6	3.41	0.10	1.08	0.06	8104	5165	4931

Table 4 (continued)

zircon grain[a]	$^{238}U/^{232}Th$	$\pm^{238}U/^{232}Th$	$^{230}Th/^{232}Th$	$\pm^{230}Th/^{232}Th$	model age (years)	model error (+ years)	model error (− years)
7	3.66	0.11	1.19	0.06	12111	5016	4795
7500 BP							
1	2.51	0.08	1.14	0.05	17667	8525	7905
2	4.55	0.14	1.87	0.08	33596	5349	5098
3	3.54	0.11	1.40	0.07	22773	6062	5742
4	1.90	0.06	1.15	0.03	31008	15073	13236
5	3.65	0.11	1.77	0.09	41624	8275	7689
6	3.13	0.09	1.21	0.06	16089	6250	5911
7	3.63	0.11	1.50	0.07	26727	6054	5735

[a] The grain labels shown here correspond to specific analysis spots which can be seen on annotated CL images in Appendix A.

[b] Value in parentheses indicates the initial value used for each volcano. References can be seen in Table 1.

earth elements (REE) may act as tracers of the evolution of melts from which zircon grew and the mineral assemblage (s) with which they equilibrated.

Th and U Thorium and U concentrations of analyzed zircon grains (Table 5) are typically subequal and vary by more than two orders of magnitude, from ~10 to >1000 ppm (Fig. 4). Thorium-uranium ratios are all ≥0.3 and reach 2, typical for magmatic zircon (e.g. Hoskin and Schaltegger 2003). Uranium and Th concentrations fall within an extended but very well-defined linear array with a slope slightly greater than 1 (Fig. 4; Th/U <1 at low concentrations, >1 at highest concentrations). While data from each eruption plot as part of the same general trend, U and Th concentrations in zircon from each eruption form distinct sub-arrays. Distinctive dark cores in Öræfajökull and Torfajökull are enriched in U and Th by an order of magnitude relative to the surrounding grain, and also have higher Th/U ratios.

Ti and Hf concentrations and the Ti vs Hf relationship Hafnium concentrations in zircon (Table 5) are relatively low, ranging from about 6000 to 11000 ppm, with a great majority falling between 7000 and 10000 (cf. Grimes et al. 2007 and Discussion, this study). Measured Ti concentrations are relatively high, with most exceeding 10 ppm and the highest concentrations exceeding 30 ppm (cf. Claiborne et al. 2006, 2010a,b; Fu et al. 2008).

With the exception of Öræfajökull and interesting inter-population relationships at Torfajökull, zircon analyses from each volcano cluster in a distinct, sub-parallel, linear array with a negative slope on plots of Ti vs Hf concentration (Fig. 5a). Within these sub-parallel groupings, Askja zircon have the highest Ti (e.g. 25 ppm at 9000 ppm Hf), followed by Torfajökull (20 ppm at 9000 ppm) and then Hekla (12 ppm at 9000 ppm).

The prehistoric 3100 BP Torfajökull dataset forms a tight cluster at relatively high Ti (17–25 ppm) and low Hf (8000–9000 ppm), while the historic 871 AD and 1477 AD eruptions plot in overlapping linear arrays that trend from compositions like those of 3100 BP to lower Ti and higher Hf (~10 ppm, 10000 ppm). The 7500 BP dataset is displaced toward lower Hf and is overall far more scattered and exhibits no identifiable inter-element trend.

The Öræfajökull dataset is unlike all other samples, with data points forming a sub-horizontal array that plot that spans a wide range of Hf concentrations (from 6000–9000 ppm), but plots (mostly) in a narrow range of Ti concentrations (~9–14 ppm).

Estimated growth temperatures from Ti concentrations Estimated zircon growth temperatures (Ferry and Watson 2007) for 158 analyses fall in the range of 730–930°C (mean 823°C; standard deviation 39°C). Individual eruptions have distinctly different Ti-in-zircon temperature distributions (Fig. 5a,b). Askja has the highest estimated temperatures with a mean of 874°C (σ=17°C), which is 60°C higher than the calculated zircon saturation temperature for our analyzed sample. The Hekla temperature distribution is similar to the distribution of the entire dataset with a mean estimated temperature of 817°C (σ=39°C), 100°C lower than the zircon saturation temperature for the Hekla sample. The temperature range recorded in Öræfajökull zircon is narrower than those from other eruptions. The mean estimated temperature at Öræfajökull is 802°C (σ=29°C), 130°C below the zircon saturation temperature.

The average estimated temperature for Torfajökull zircon (prehistoric and historic) is the same as that for our total Iceland zircon set, but the temperature distribution is skewed to slightly lower temperatures. Zircon populations from individual eruptions have distinct Ti-temperature distributions. The mean estimated temperature from the 1477 AD eruption is 831°C (σ=23°C), 60°C lower than the zircon saturation T. The 871 AD Torfajökull temperature distribution spans a far narrower range of temperatures than the total Icelandic compilation. The

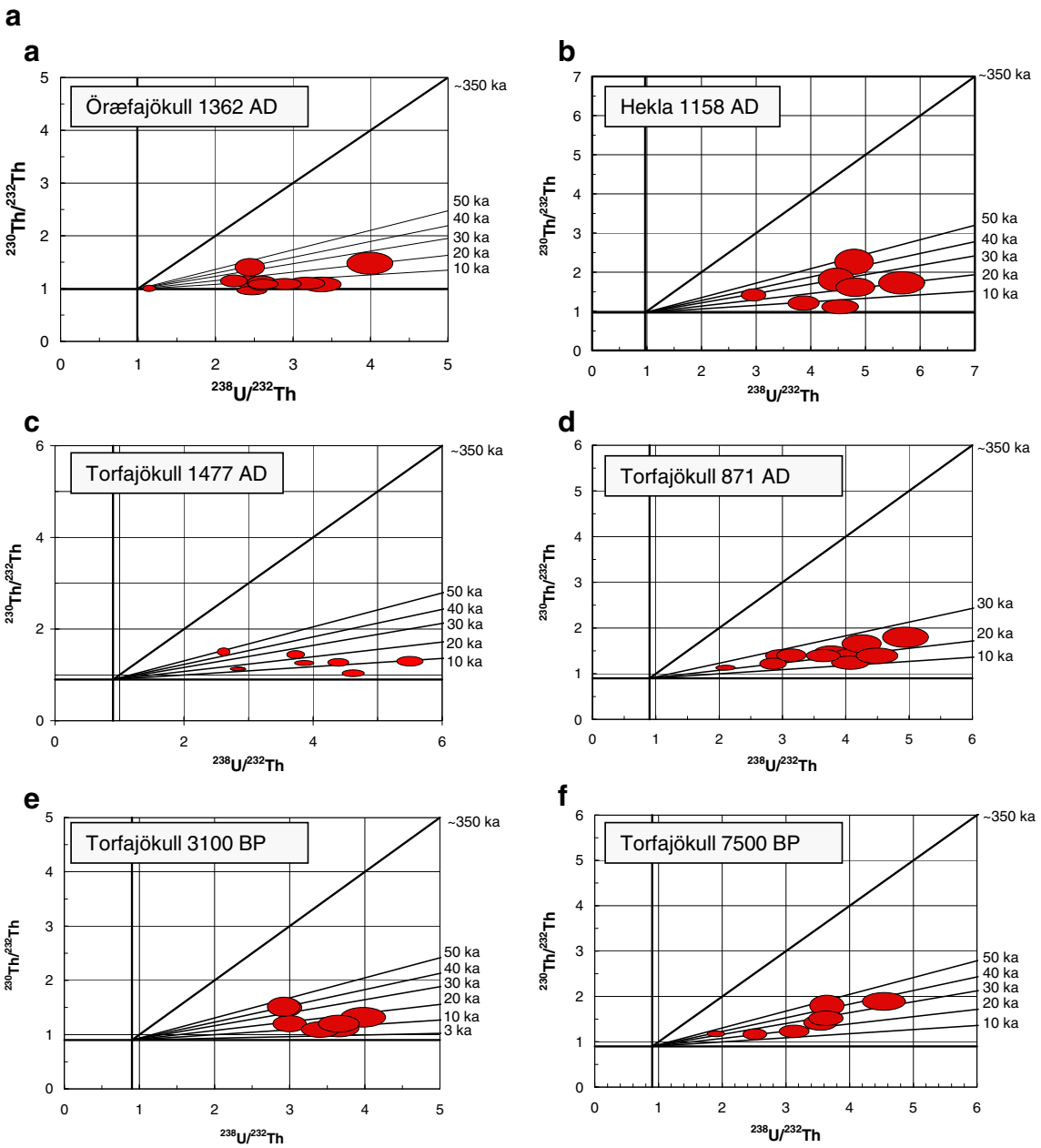

Fig. 3 **a**: ($^{230}Th/^{232}Th$) vs ($^{238}U/^{232}Th$) activity diagrams for analyzed samples. Reference isochrons, drawn at 10 ka intervals, intersect equiline at estimated initial ($^{230}Th/^{232}Th$) from which model ages were estimated (see Table 1). A: Öræfajökull; B: Hekla; C: Torfajökull 1477 AD; D; Torfajökull 871 AD; E: Torfajökull 3100 BP; F: Torfajökull 7500 BP. **b**: Probability density curves for model ages derived using U-Th disequilibrium dating techniques (Lowenstern et al. 2000; Charlier et al. 2005). A: Öræfajökull; B: Hekla; C: Torfajökull 1477 AD; D; Torfajökull 871 AD; E: Torfajökull 3100 BP; F: Torfajökull 7500 BP. Initial ($^{230}Th/^{232}Th$) ratios for each eruptive deposit were taken from published literature and can be found in Table 1

mean estimated temperature for 871 AD is 824°C (σ=20°C), 55°C below the zircon saturation T. Estimated growth temperatures for zircon from the 3100 BP eruption at Torfajökull define a relatively narrow temperature range (800–900°C) with a mean of 859°C (σ=12°C), 60°C lower than the zircon saturation T. Estimated temperatures from the 7500 BP eruption are relatively low, with a mean of 795°C (σ=39°C), 125°C lower than the zircon saturation T for this sample.

Rare Earth Elements (REE) Zircon from all samples show chondrite-normalized REE patterns that are broadly similar to each other and to igneous zircon in general, with concentrations increasing by about four orders of magnitude from light (L) to heavy (H) REE and positive Ce and negative Eu anomalies (Table 5, Fig. 6). Torfajökull 3100 BP and 1477 AD zircon have notably lower REE abundances than those from the 871 AD and 7500 BP

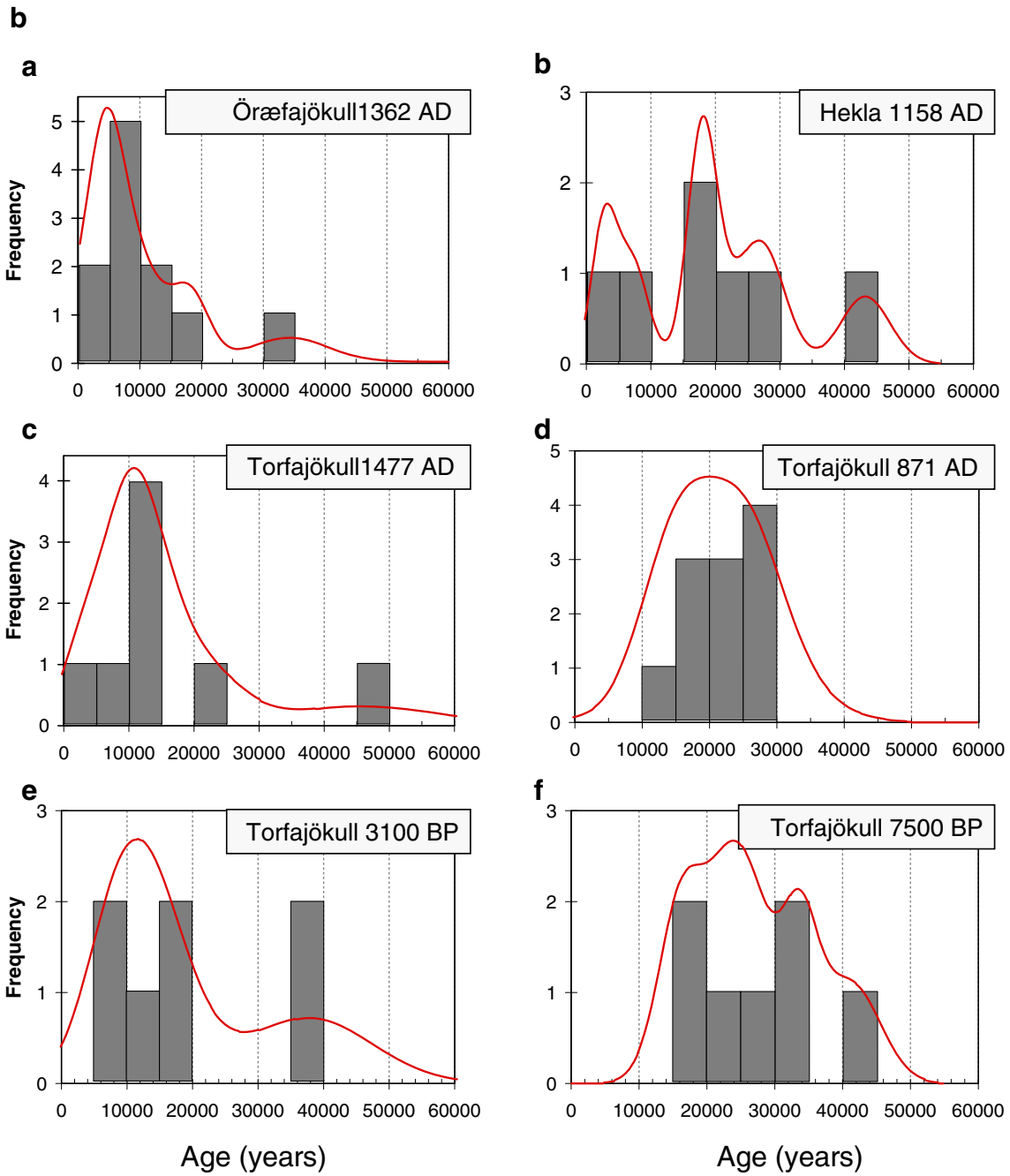

Fig. 3 (continued)

eruptions, and Öræfajökull zircon may be divided into two distinct groupings with patterns of similar shape but different absolute abundances.

To emphasize the population-to-population and grain-to-grain REE variability we also plot the ratio Yb/Nd vs Hf (concentrations, not chondrite normalized) to show relative enrichment of HREE relative to LREE (Fig. 7). Overall, there is a positive correlation between Yb/Nd (HREE/LREE) and Hf, indicating enrichment in HREE relative to LREE with increasing fractionation (Fig. 7), shown most clearly by zircon from the Torfajökull 7500 BP lava. The trend established by Torfajökull 7500 BP seems to continue to higher levels of fractionation (higher Hf) in Torfajökull 3100 BP and Torfajökull 1477 AD. Öræfajökull also displays the shallow positive sloping trend at lower degrees of fractionation (lower Hf), but at approximately 8000 ppm there is a sudden break in slope, and the enrichment of HREE relative to LREE becomes much more pronounced.

Table 5 SHRIMP trace element analyses of individual zircon grains(ppm)

Label[a]	grain location	Ti	Y	Nb	Hf	Th	U	La	Ce	Nd	Sm	Eu	Gd	Tb	Dy	Ho	Er	Tm	Yb	Lu
Askja 1875																				
IC45-1.1I	Interior	23.2	2109	7.2	9494	32.7	53.3	0.05	7.51	3.94	8.7	1.92	66.9	n.a.	243.4	n.a.	331.5	n.a.	421.0	62.6
IC45-1.2E	Edge	20.7	1658	5.6	9909	25.6	43.0	0.04	6.09	2.83	7.7	2.09	64.1	n.a.	222.3	n.a.	301.3	n.a.	397.7	61.5
IC45-2.1I	Interior	29.0	1700	4.3	9260	25.9	39.5	0.05	5.39	4.51	8.7	2.42	66.2	n.a.	238.1	n.a.	309.0	n.a.	406.0	62.4
IC45-2.2R	Edge	25.3	549	5.5	9101	10.3	23.3	0.04	3.34	0.51	1.6	0.53	17.0	n.a.	67.4	n.a.	105.8	n.a.	159.5	26.7
IC45-3.1C	Interior	21.3	1359	5.3	9569	25.7	43.0	0.04	5.53	2.63	6.7	1.89	56.6	n.a.	211.5	n.a.	288.7	n.a.	378.2	59.6
IC45-3.2R	Edge	24.4	1086	8.9	9178	40.1	67.9	0.03	7.04	1.49	4.1	1.10	33.8	n.a.	145.9	n.a.	215.1	n.a.	316.6	50.8
IC45-4.1R	Edge	23.2	1102	10.3	9371	40.2	65.4	0.04	7.74	1.45	3.6	1.11	34.1	n.a.	133.0	n.a.	194.5	n.a.	287.2	49.1
IC45-4.2I	Interior	19.8	1748	5.9	9684	29.3	49.1	0.04	6.43	3.18	8.8	2.17	69.5	n.a.	236.7	n.a.	320.8	n.a.	416.9	64.5
IC45-4.3R	Edge	24.2	928	8.3	9470	23.4	46.3	0.03	5.97	0.91	3.5	0.87	28.4	n.a.	121.3	n.a.	179.1	n.a.	269.8	42.2
IC45-5.1I	Interior	28.9	1551	4.3	9105	21.0	35.9	0.07	4.68	3.62	8.6	2.38	64.2	n.a.	221.0	n.a.	289.5	n.a.	383.7	60.4
IC45-5.2I	Edge	23.0	2809	11.8	8827	56.2	75.0	0.06	10.26	6.18	14.5	3.52	113.8	n.a.	373.7	n.a.	481.2	n.a.	635.3	96.1
IC45-6.2I	Interior	22.8	1244	4.9	9715	18.1	34.5	0.03	4.43	1.88	4.7	1.57	45.5	n.a.	165.2	n.a.	227.3	n.a.	317.9	50.8
IC45-7.1E	Edge	19.0	2476	10.1	9824	52.2	82.3	0.08	11.11	5.42	11.2	2.63	90.7	n.a.	310.8	n.a.	424.9	n.a.	543.8	81.6
IC45-7.2I	Interior	32.1	1432	3.8	9167	20.1	34.2	0.04	4.11	3.64	7.9	2.22	58.3	n.a.	216.9	n.a.	285.7	n.a.	388.1	58.7
IC45-8.1I	Interior	20.3	813	10.0	10094	19.0	40.9	0.03	7.46	0.60	2.3	0.69	23.2	n.a.	106.6	n.a.	159.7	n.a.	246.5	37.7
IC45-9.1I	Interior	22.6	1850	5.4	9427	28.7	47.3	0.07	6.47	4.43	9.9	2.35	71.2	n.a.	245.6	n.a.	334.2	n.a.	434.3	66.0
Hekla 1158 AD																				
IHB1-1.1I	Interior	18.9	3573	12.6	8129	117.9	175.9	0.05	12.29	6.97	17.7	6.36	130.7	n.a.	492.7	n.a.	711.7	n.a.	1066.8	171.3
IHB1-10.1I	Interior	10.3	1527	7.5	9533	41.2	92.8	0.04	5.79	1.97	5.4	1.63	46.8	n.a.	182.6	n.a.	288.4	n.a.	452.6	79.4
IHB1-11.1I	Interior	17.3	2678	9.1	8208	79.3	131.4	0.10	8.54	5.47	12.7	4.39	97.6	n.a.	369.9	n.a.	532.3	n.a.	802.3	128.0
IHB1-12.1R	Edge	13.0	988	9.9	9468	47.4	109.6	0.02	7.22	0.81	2.4	0.86	22.7	n.a.	108.6	n.a.	186.4	n.a.	313.7	53.6
IHB1-12.2C	Core	14.6	6523	30.1	8207	308.5	313.0	0.15	40.72	15.20	37.9	13.11	272.4	n.a.	918.9	n.a.	1229.1	n.a.	1734.9	282.3
IHB1-13.1I	Interior	8.4	1669	10.4	9712	103.7	143.0	0.04	16.64	2.58	6.9	3.11	68.2	n.a.	319.2	n.a.	494.6	n.a.	778.9	128.7
IHB1-14.1I	Interior	7.4	1972	8.9	8502	46.4	101.4	0.06	9.70	3.31	7.5	2.27	65.9	n.a.	257.6	n.a.	378.8	n.a.	512.2	77.4
IHB1-14.2R	Edge	36.5	1225	18.2	10466	45.1	107.9	0.18	10.29	1.04	3.0	0.71	28.8	n.a.	144.4	n.a.	255.6	n.a.	426.6	69.8
IHB1-15.1I	Edge	15.8	1723	5.6	9272	41.4	81.1	0.11	5.71	2.52	6.5	2.21	52.1	n.a.	202.0	n.a.	308.3	n.a.	477.8	80.2
IHB1-16.1I	Interior	18.5	5123	26.3	8088	136.1	194.2	0.15	20.70	10.28	23.7	7.46	165.2	n.a.	590.6	n.a.	815.4	n.a.	1184.3	190.5
IHB1-17.1I	Interior	11.0	1781	5.3	9293	45.9	94.2	0.05	5.70	2.32	6.3	2.19	53.6	n.a.	223.3	n.a.	348.3	n.a.	539.0	86.9
IHB1-18.1I	Interior	10.3	1759	5.0	9477	41.8	86.4	0.03	5.20	2.17	6.2	2.03	52.8	n.a.	209.5	n.a.	319.2	n.a.	490.7	80.3
IHB1-19.1I	Interior	10.0	1643	5.3	9421	41.1	83.1	0.10	5.83	2.03	5.8	1.96	50.1	n.a.	195.3	n.a.	297.5	n.a.	468.9	73.9
IHB1-2.1I	Interior	10.2	1741	5.4	9479	48.3	96.5	0.03	5.79	2.22	6.2	2.18	52.2	n.a.	226.2	n.a.	348.8	n.a.	541.9	87.7
IHB1-20.1I	Interior	29.6	1627	6.2	9149	37.1	77.8	0.67	6.90	2.22	5.6	1.79	47.8	n.a.	190.5	n.a.	290.0	n.a.	459.4	76.0
IHB1-21.2T	Edge	10.9	1323	5.1	9329	38.0	82.6	0.03	5.21	1.56	4.7	1.57	39.8	n.a.	175.2	n.a.	280.8	n.a.	446.8	74.5
IHB1-22.1I	Interior	19.7	7090	36.1	7889	298.4	319.0	0.09	28.74	15.09	38.9	13.08	288.1	n.a.	1016.2	n.a.	1358.6	n.a.	1901.9	298.1

Table 5 (continued)

Label[a]	grain location	Ti	Y	Nb	Hf	Th	U	La	Ce	Nd	Sm	Eu	Gd	Tb	Dy	Ho	Er	Tm	Yb	Lu
IHB1-22.2I	Edge	14.8	2523	8.5	8666	72.6	133.8	0.06	7.96	4.54	11.6	4.08	89.9	n.a.	358.7	n.a.	507.8	n.a.	770.6	122.8
IHB1-23.1I	Interior	15.1	5032	23.8	8522	239.8	324.2	0.08	18.98	7.28	20.9	6.84	176.5	n.a.	718.9	n.a.	1016.0	n.a.	1521.0	242.7
IHB1-24.1I	Interior	22.1	2199	15.2	8185	69.7	130.6	0.10	8.67	2.37	7.3	2.69	63.1	n.a.	277.5	n.a.	430.7	n.a.	690.4	115.6
IHB1-3.1I	Interior	12.7	2367	7.9	9058	91.5	145.3	0.05	6.35	2.94	9.4	3.41	86.0	n.a.	347.1	n.a.	517.9	n.a.	793.8	129.1
IHB1-4.1I	Interior	17.2	2999	10.7	8636	86.1	142.7	0.08	8.51	6.10	14.1	4.63	109.3	n.a.	379.2	n.a.	548.8	n.a.	816.1	137.2
IHB1-5.1I	Interior	11.1	1786	5.7	9389	51.4	104.5	0.05	6.08	2.58	6.1	1.92	53.2	n.a.	228.2	n.a.	353.8	n.a.	530.3	88.9
IHB1-6.1C	Interior	14.8	677	7.7	8454	14.8	37.6	0.04	7.65	0.79	2.3	0.70	19.6	n.a.	78.7	n.a.	132.6	n.a.	212.2	36.8
IHB1-6.2R	Edge	12.9	625	5.5	9794	22.5	69.9	0.03	4.76	0.42	1.8	0.62	15.6	n.a.	78.3	n.a.	138.3	n.a.	246.1	41.9
IHB1-7.1I	Interior	10.0	1762	6.4	10553	42.7	86.3	0.05	6.27	2.46	6.2	2.13	57.7	n.a.	215.7	n.a.	323.9	n.a.	502.9	86.4
IHB1-8.1T	Edge	14.0	1403	19.0	9763	198.6	271.2	1.90	17.94	4.06	4.7	1.57	42.3	n.a.	198.6	n.a.	336.9	n.a.	570.7	96.3
IHB1-9.1I	Interior	13.0	2301	7.6	8883	74.0	123.7	0.05	6.21	2.85	8.6	3.22	75.7	n.a.	281.4	n.a.	433.3	n.a.	673.5	113.5
IHB1-9.2R	Edge	17.8	2467	7.5	8387	67.9	112.5	0.07	7.25	4.55	11.3	4.09	87.6	n.a.	325.9	n.a.	463.6	n.a.	723.8	120.2
Öræfajökull 1362 AD																				
IOHN1-1.2E	Interior	12.4	5832	24.2	6211	135.1	174.3	0.07	25.28	9.82	26.7	10.65	219.1	n.a.	773.3	n.a.	1043.7	n.a.	1377.6	210.8
IOHN1-10.1I	Interior	8.8	1032	5.0	8663	16.5	38.3	0.04	5.20	0.96	3.2	1.17	28.5	n.a.	121.2	n.a.	193.3	n.a.	291.6	47.0
IOHN1-11.1I	Edge	9.5	1369	15.2	8127	45.9	89.2	0.03	16.82	1.43	4.6	1.07	39.4	n.a.	177.3	n.a.	269.0	n.a.	389.6	59.5
IOHN1-13.1I	Interior	9.8	1684	5.2	8309	35.0	66.8	0.05	6.28	2.16	6.6	2.16	55.1	n.a.	229.1	n.a.	331.9	n.a.	480.0	73.3
IOHN1-14.1I	Interior	8.9	1757	6.9	8133	33.2	62.3	0.04	6.42	2.06	6.1	1.98	59.8	n.a.	216.4	n.a.	329.3	n.a.	472.3	76.0
IOHN1-14.2E	Edge	11.6	741	6.3	7723	14.2	43.5	0.04	4.36	0.55	2.0	0.62	17.4	n.a.	87.3	n.a.	144.9	n.a.	239.8	38.9
IOHN1-15.2I	Interior	13.0	820	7.3	8396	24.0	57.8	0.05	5.73	0.67	2.2	0.73	19.9	n.a.	89.7	n.a.	152.3	n.a.	235.6	40.9
IOHN1-15.3C	Core	16.9	18199	203.8	7744	1040.0	887.3	0.24	326.59	26.25	70.0	9.80	608.9	n.a.	2330.5	n.a.	3190.5	n.a.	3966.4	549.8
IOHN1-16.1I	Interior	9.2	6952	44.8	7868	274.6	322.1	0.12	60.16	9.92	28.8	6.17	251.6	n.a.	877.0	n.a.	1211.8	n.a.	1597.2	236.7
IOHN1-17.1E	Interior	11.7	824	6.9	8150	29.6	63.1	0.04	6.63	0.71	2.3	0.82	21.6	n.a.	103.0	n.a.	167.2	n.a.	266.7	42.9
IOHN1-17.2C	Core	9.2	9131	56.5	7339	308.9	371.1	0.12	87.97	14.52	40.1	10.04	326.6	n.a.	1238.5	n.a.	1705.1	n.a.	2207.4	321.4
IOHN1-18.1E	Edge	14.6	991	9.0	8047	40.1	78.8	0.02	7.53	0.77	2.8	0.97	25.5	n.a.	123.7	n.a.	201.5	n.a.	321.7	49.7
IOHN1-19.1C	Core	10.6	5234	62.3	8110	367.7	389.5	0.38	69.57	6.17	18.9	3.79	176.5	n.a.	694.4	n.a.	984.7	n.a.	1286.4	194.0
IOHN1-19.2T2	Edge	12.0	1027	8.4	7627	29.8	65.5	0.04	7.66	0.95	2.9	0.97	25.2	n.a.	118.6	n.a.	192.3	n.a.	297.9	48.6
IOHN1-2.1R	Edge	11.6	921	8.0	8567	23.8	58.7	0.04	6.44	0.66	2.0	0.88	21.0	n.a.	97.0	n.a.	171.7	n.a.	269.1	43.8
IOHN1-3.1T	Edge	11.6	7104	40.4	7294	203.8	241.3	0.08	37.03	9.32	30.2	9.87	252.6	n.a.	946.2	n.a.	1283.3	n.a.	1697.2	254.6
IOHN1-3.2I	Interior	12.0	8016	44.8	7019	257.9	277.4	0.13	50.09	13.30	36.1	11.96	315.4	n.a.	1070.7	n.a.	1448.7	n.a.	1852.1	280.0
IOHN1-4.1C	Core	29.1	18996	166.4	7336	893.3	761.4	0.32	351.38	37.51	93.0	12.34	689.4	n.a.	2577.6	n.a.	3344.6	n.a.	4104.4	570.2
IOHN1-4.2R	Edge	12.8	1558	22.7	8982	119.9	147.0	0.04	16.31	1.17	4.3	1.23	41.5	n.a.	170.6	n.a.	262.8	n.a.	391.1	65.1
IOHN1-5.1C	Core	20.3	12297	772.2	9008	1494.9	1593.0	0.22	357.54	8.90	25.0	4.03	232.8	n.a.	1360.5	n.a.	2290.2	n.a.	3489.5	491.4
IOHN1-5.2T	Edge	12.8	914	8.2	8183	28.6	63.3	0.03	6.79	0.70	2.1	0.81	22.7	n.a.	104.4	n.a.	176.6	n.a.	278.9	45.1
IOHN1-7.1T	Edge	12.7	978	8.7	7908	33.9	71.2	0.02	7.31	0.91	2.6	0.88	24.0	n.a.	113.0	n.a.	185.0	n.a.	294.9	46.6

Table 5 (continued)

Label[a]	grain location	Ti	Y	Nb	Hf	Th	U	La	Ce	Nd	Sm	Eu	Gd	Tb	Dy	Ho	Er	Tm	Yb	Lu
IOHN1-7.2C	Core	12.4	12592	88.2	7471	583.4	554.2	0.18	104.52	22.48	59.4	12.11	487.0	n.a.	1684.5	n.a.	2242.5	n.a.	2842.0	422.9
IOHN1-8.1I	Interior	12.6	1140	5.6	8985	28.2	51.1	0.11	6.46	1.02	3.2	1.04	31.7	n.a.	132.0	n.a.	205.7	n.a.	341.8	53.9
IOHN1-9.1E	Edge	11.8	5106	20.6	6718	126.6	173.8	0.08	22.28	8.21	22.5	8.67	188.2	n.a.	655.9	n.a.	890.4	n.a.	1204.1	189.2
Torfajökull 1477 AD																				
ITN1-1.1I	Interior	19.2	801	9.5	9168	56.1	84.9	0.06	20.84	0.88	2.4	0.69	20.8	n.a.	87.7	n.a.	144.7	n.a.	244.0	39.7
ITN1-10.1I	Interior	12.2	2588	13.9	9310	160.0	221.4	0.04	23.31	5.13	10.2	1.59	74.7	n.a.	326.1	n.a.	484.5	n.a.	728.5	109.1
ITN1-11.1I	Interior	15.9	1727	8.2	9579	83.1	112.3	0.07	17.96	3.41	7.0	1.66	55.5	n.a.	198.3	n.a.	293.4	n.a.	431.0	71.3
ITN1-12.1I	Interior	19.1	2578	12.9	8832	150.9	178.0	0.09	26.67	4.94	11.0	2.80	86.7	n.a.	342.4	n.a.	494.4	n.a.	728.5	112.3
ITN1-14.1E	Edge	16.3	915	9.7	9535	63.9	112.7	0.03	18.37	1.11	3.0	0.77	22.6	n.a.	108.7	n.a.	175.6	n.a.	295.0	46.8
ITN1-14.2I	Interior	19.4	1631	12.9	8858	109.4	152.6	0.03	26.10	3.11	6.2	1.60	45.8	n.a.	216.2	n.a.	334.8	n.a.	501.4	81.1
ITN1-2.1I	Interior	18.4	2376	43.9	9058	179.9	300.6	0.05	46.68	2.69	6.1	1.32	54.8	n.a.	261.3	n.a.	467.8	n.a.	785.5	130.0
ITN1-3.1T	Edge	21.3	1741	22.6	9064	308.6	277.9	0.04	39.12	2.56	5.6	1.30	50.2	n.a.	211.7	n.a.	331.2	n.a.	519.6	82.5
ITN1-4.1T	Edge	21.8	1191	14.1	8882	149.1	183.8	0.04	25.23	1.67	3.9	0.98	30.6	n.a.	144.0	n.a.	230.3	n.a.	375.9	59.4
ITN1-5.1E	Edge	15.1	1217	17.0	9541	133.1	196.2	0.03	25.63	1.50	3.4	0.70	30.1	n.a.	138.2	n.a.	223.8	n.a.	359.3	57.4
ITN1-5.2C	Core	10.2	8213	184.2	8942	1682.9	1943.4	0.13	166.91	12.37	29.3	0.84	238.0	n.a.	1169.6	n.a.	1812.8	n.a.	2717.7	391.7
ITN1-6.1C	Interior	12.4	3135	17.7	9472	171.8	225.0	0.09	26.60	5.46	11.8	2.11	96.8	n.a.	363.0	n.a.	520.1	n.a.	740.9	115.7
ITN1-6.2E	Edge	14.4	852	10.7	9879	75.0	106.7	0.03	18.94	0.88	2.2	0.51	20.3	n.a.	93.9	n.a.	156.6	n.a.	265.4	42.6
ITN1-7.1I	Interior	16.6	3086	28.1	9482	203.9	267.4	0.08	38.07	5.01	11.2	2.37	95.3	n.a.	381.3	n.a.	572.5	n.a.	854.4	137.2
ITN1-8.1E	Edge	17.2	1741	27.2	9003	245.0	286.2	0.06	37.33	2.33	5.7	1.03	46.1	n.a.	214.6	n.a.	335.0	n.a.	519.0	81.9
ITN1-8.2I	Interior	12.5	2085	29.7	9318	143.6	233.8	0.04	30.09	2.47	5.9	1.10	57.3	n.a.	219.4	n.a.	367.6	n.a.	599.0	98.2
ITN1-9.2E	Edge	16.8	1109	12.3	8955	72.5	115.3	0.04	24.91	1.44	3.0	0.91	28.4	n.a.	129.6	n.a.	202.0	n.a.	324.2	52.3
Torfajökull 871 AD																				
ITHN1-1.1E	Edge	12.7	3136	23.6	9151	218.8	263.0	0.14	29.60	6.45	11.9	2.18	104.1	34.7	368.3	136.4	552.2	106.3	787.0	128.3
ITHN1-1.2I	Interior	17.6	1845	34.0	8964	292.7	295.3	0.04	42.93	2.66	6.0	1.15	53.7	18.8	208.0	75.3	321.3	62.5	475.5	77.5
ITHN1-2.1C	Core	20.6	6651	62.0	8763	612.6	598.8	9.13	116.95	19.14	33.5	4.21	256.6	80.6	828.0	290.4	1143.1	217.1	1576.6	250.0
ITHN1-2.2E	Edge	17.8	1878	34.7	9482	211.5	261.7	0.04	46.70	2.68	6.2	1.17	57.7	19.8	213.2	79.2	330.9	66.3	497.8	82.8
ITHN1-3.1I	Interior	11.2	2012	17.5	9220	113.8	96.5	0.06	23.33	4.20	8.1	1.49	68.0	21.5	231.5	83.7	334.4	64.6	484.9	78.1
ITHN1-3.2DZ	Edge	12.3	3981	170.9	9481	801.2	908.5	0.11	142.42	5.01	12.3	1.18	119.6	43.0	460.8	169.4	708.4	138.6	1068.7	167.6
ITHN1-4.1C	Core	13.7	8457	391.3	9379	3829.0	2277.8	0.26	380.37	13.88	31.5	2.14	281.2	102.2	1066.6	364.5	1498.5	277.5	2082.3	296.1
ITHN1-4.2E	Edge	15.8	1859	37.4	9096	317.6	320.8	0.07	45.72	2.70	6.0	1.05	53.4	18.8	202.9	76.9	315.4	62.9	471.1	75.5
ITHN1-5.1I	Edge	14.8	3012	32.0	9020	234.9	277.5	0.12	37.81	5.32	10.9	2.12	101.2	32.0	350.2	129.6	524.8	100.6	765.8	122.8
ITHN1-6.1I	Interior	18.8	2125	41.4	8615	730.9	503.2	0.03	53.75	3.40	6.7	1.26	62.4	21.9	237.9	90.1	372.1	69.9	538.8	87.1
ITHN1-6.2E	Edge	13.0	3441	28.6	8854	258.7	299.7	0.11	33.69	6.48	12.7	2.55	117.4	39.4	413.5	147.7	603.1	113.4	851.7	136.8
ITHN1-7.1I	Interior	13.1	2303	22.6	9276	149.9	202.3	0.37	27.82	5.19	8.9	1.59	72.8	24.5	260.5	96.6	398.1	75.5	573.9	92.7
ITHN1-8.1E	Edge	20.8	2413	20.0	9339	159.0	194.4	0.14	29.21	4.78	8.9	2.02	77.9	26.4	288.4	102.9	428.5	81.8	635.3	101.7

Table 5 (continued)

Label[a]	grain location	Ti	Y	Nb	Hf	Th	U	La	Ce	Nd	Sm	Eu	Gd	Tb	Dy	Ho	Er	Tm	Yb	Lu
ITHN1-9.1C	Core	14.5	4990	53.0	9194	406.5	474.6	0.36	66.70	9.33	19.8	1.72	168.2	56.6	584.8	212.1	854.2	162.0	1208.3	195.0
ITHN1-9.2I	Interior	14.3	2094	49.1	9565	456.8	476.8	0.06	59.35	3.03	7.5	0.86	65.8	22.3	243.3	88.8	370.7	70.9	558.1	88.9
ITHN1-9.3T	Edge	16.0	1886	40.1	9408	415.5	404.3	0.06	48.15	2.58	5.9	1.02	54.7	19.4	207.7	77.9	320.8	63.3	488.4	78.7
ITHN1-9.4I	Interior	14.7	1419	30.0	9233	192.0	247.0	0.04	34.48	1.88	4.6	0.67	39.0	13.8	150.6	58.3	239.5	48.2	369.9	62.3
Torfajökull 3100 BP																				
3A03TE-1.1I	Interior	20.8	1340	30.6	8993	128.8	158.8	0.14	23.58	5.24	10.9	2.79	98.7	32.4	331.0	119.8	480.5	92.9	688.7	113.7
3A03TE-1.2T	Edge	19.5	940	22.4	8627	97.9	131.6	0.03	21.88	1.53	3.3	0.87	31.8	11.3	122.4	47.9	212.3	43.1	334.7	59.0
3A03TE-8.1I	Interior	20.3	2970	36.6	8263	210.3	236.2	0.03	16.19	1.64	3.3	0.93	29.5	10.4	118.1	44.6	191.9	37.4	292.0	49.1
3A03TE-3.1I	Interior	22.5	2493	47.7	8195	192.2	253.5	0.15	30.83	6.68	14.0	3.33	110.8	36.0	374.6	136.5	529.5	101.7	774.4	121.8
3A03TE-2.1I	Interior	23.4	2030	35.1	8250	155.6	199.0	0.02	24.89	1.76	4.1	0.96	34.1	11.3	127.3	48.9	210.4	41.8	320.3	54.5
3A03TE-9.1C	Core	22.7	2607	40.4	8899	392.3	318.1	0.03	19.53	1.15	3.3	0.79	26.9	9.2	99.9	38.8	167.5	33.3	260.1	45.1
3A03TE-4.1E	Edge	17.8	1237	21.5	8334	99.7	142.1	0.03	20.71	1.51	2.7	0.71	27.4	9.8	106.4	40.4	173.6	34.0	266.2	46.1
3A03TE-10.1I	Interior	21.1	2102	40.6	8659	189.0	254.5	0.12	37.21	4.76	10.9	2.74	95.2	31.3	332.2	124.5	516.4	100.7	763.4	126.1
3A03TE-5.1E	Edge	25.7	1546	29.0	8709	358.7	283.7	0.17	34.43	6.18	13.3	3.31	114.2	37.9	386.4	138.1	560.0	109.0	806.6	130.9
3A03TE-6.1E	Edge	20.6	3272	32.6	8873	226.4	245.6	0.06	26.37	2.28	4.3	1.15	36.3	13.1	146.1	55.9	234.6	46.2	362.3	61.6
3A03TE-7.1E	Edge	21.0	2387	31.3	8135	231.4	220.0	0.13	39.56	4.48	8.8	2.17	75.0	25.7	271.2	98.5	414.3	78.4	606.2	100.0
3A03TE-11.1E	Edge	18.6	1099	16.2	7899	126.5	162.0	0.04	32.73	2.61	5.5	1.46	51.1	18.6	212.2	83.8	385.8	76.8	614.8	106.1
3A03TE-12.1I	Edge	19.6	979	22.1	8997	97.0	131.3	0.02	25.79	1.95	3.5	0.94	32.0	11.9	133.0	53.4	232.1	47.3	374.3	65.7
3A03TE-13.1E	Edge	21.1	1307	24.5	8546	143.6	182.9	0.04	28.94	2.03	4.3	1.10	37.2	13.5	142.1	54.8	226.9	43.6	342.4	57.6
3A03TE-14.1E	Edge	22.5	1413	28.7	8574	274.7	248.6	0.03	28.35	2.33	4.6	1.05	37.9	14.4	153.1	56.2	247.3	49.1	371.2	61.2
3A03TE-15.1E	Edge	21.2	1343	26.1	8413	202.3	193.2	0.08	40.72	3.24	6.1	1.48	56.6	20.3	235.2	96.4	425.8	86.1	660.9	113.3
3A03TE-16.1C	Interior	18.7	3240	28.1	8560	202.5	220.8	0.10	49.24	4.58	9.8	2.12	84.0	28.4	298.2	108.1	444.6	85.1	615.0	101.5
3A03TE-17.1C	Interior	19.4	1195	25.0	8794	150.3	156.2	0.07	36.22	3.18	6.2	1.54	53.8	18.0	202.7	80.9	356.4	71.3	571.9	96.8
3A03TE-18.1I	Interior	17.0	2869	23.3	8517	175.6	207.2	0.04	32.58	2.60	4.9	1.20	43.1	14.9	164.9	62.9	269.1	53.1	415.8	69.9
Torfajökull 7500 BP																				
5A03TE-1.1	Core	15.7	4927	146.6	6815	1413.7	812.3	0.11	342.74	8.71	22.4	5.77	209.0	67.0	658.2	218.3	837.5	145.7	1014.4	149.2
5A03TE-10.1I	Edge	31.9	4528	31.5	7310	297.0	279.7	0.23	29.66	15.43	27.9	10.05	191.3	56.2	545.1	192.0	754.4	145.5	1076.0	178.9
5A03TE-11.1I	Interior	9.1	1479	38.7	7111	110.6	146.7	0.01	56.94	2.37	5.0	1.29	49.8	16.8	178.1	66.4	270.6	49.6	364.1	57.5
5A03TE-12.1C	Interior	14.3	1883	38.6	8470	300.5	254.4	0.06	55.41	3.16	6.3	1.87	61.2	21.0	226.0	81.0	340.0	63.7	478.7	78.6
5A03TE-13.1I	Interior	14.3	2380	37.8	7655	146.9	143.8	0.14	79.39	4.64	10.1	2.81	79.7	28.1	283.6	101.7	422.4	76.8	566.3	94.5
5A03TE-14.1I	Interior	17.5	3689	29.2	7382	463.9	497.5	0.16	27.55	10.35	19.0	4.75	133.7	42.5	431.1	151.0	626.1	124.8	977.9	161.3
5A03TE-15.1I	Interior	7.7	3197	33.3	7666	119.5	165.4	0.14	45.24	5.66	13.0	3.20	117.6	39.1	400.2	142.2	555.1	101.3	696.2	112.7
5A03TE-15.2E	Edge	8.1	1438	41.1	8967	145.1	223.4	0.04	51.13	2.03	4.7	0.86	41.4	15.3	162.2	61.4	259.0	50.1	363.3	58.0
5A03TE-16.1C	Interior	8.5	3103	52.0	6808	122.5	169.7	0.10	59.01	5.36	11.8	3.09	105.7	34.5	367.1	131.7	524.7	96.4	712.5	112.1
5A03TE-17.1C	Core	13.9	6652	126.6	9084	2165.9	1404.4	0.37	223.41	13.98	29.2	5.36	251.6	86.7	891.7	310.5	1263.8	238.1	1731.7	265.9

Table 5 (continued)

Label[a]	grain location	Ti	Y	Nb	Hf	Th	U	La	Ce	Nd	Sm	Eu	Gd	Tb	Dy	Ho	Er	Tm	Yb	Lu
5A03TE-18.1I	Interior	10.3	1837	46.9	7723	200.9	229.8	0.04	74.83	2.63	6.2	1.51	61.1	21.3	223.3	78.9	318.2	59.6	431.6	68.2
5A03TE-19.1I	Interior	12.5	1256	22.6	8710	56.2	85.9	0.03	16.44	2.49	4.8	1.46	45.8	14.6	159.6	55.3	231.5	43.6	337.9	54.6
5A03TE-2.1I	Interior	5.9	5397	64.0	7753	231.1	314.4	0.11	92.16	10.97	24.9	6.94	206.3	69.6	720.3	246.9	967.1	173.7	1210.9	184.7
5A03TE-2.2E	Edge	10.7	1404	115.1	11335	339.0	321.2	0.11	55.24	2.22	5.2	1.24	41.6	16.9	183.7	63.2	281.8	55.8	437.5	65.3
5A03TE-20.1I	Interior	22.9	2511	34.3	7521	346.8	317.1	0.09	30.90	4.14	8.8	2.81	74.7	26.4	264.8	103.6	416.5	79.8	592.9	99.8
5A03TE-21.1E	Edge	8.9	2112	60.5	8253	313.1	345.2	0.05	84.95	3.19	6.8	1.47	66.6	22.7	243.7	92.3	354.2	68.3	486.8	76.0
5A03TE-21.2C	Interior	14.9	2348	65.0	7525	383.5	393.1	1.05	101.81	4.15	8.5	1.95	75.6	27.1	279.1	99.5	395.0	73.5	512.7	83.1
5A03TE-22.1C	Core	17.2	6587	220.3	7442	1133.7	502.1	0.67	886.12	16.01	34.0	7.67	268.4	82.9	833.2	295.8	1104.5	196.4	1363.7	199.3
5A03TE-22.2E	Edge	12.1	1893	52.4	8389	326.6	313.2	0.03	67.57	2.88	6.5	1.63	60.9	21.1	218.4	81.7	325.3	59.9	442.3	71.3
5A03TE-23.1E	Edge	21.8	4555	36.4	7374	302.8	327.4	0.24	31.91	14.99	27.9	8.53	192.9	58.8	575.4	199.8	781.6	149.9	1079.3	179.0
5A03TE-24.1C	Interior	8.1	3909	49.8	7514	221.1	264.1	0.14	87.46	6.49	17.8	4.09	155.1	49.8	509.3	177.0	695.6	127.8	892.3	138.8
5A03TE-24.2E	Edge	9.8	2680	70.9	7982	365.6	387.3	0.04	114.14	3.68	8.4	1.82	93.2	30.2	321.5	115.4	452.9	82.9	608.6	96.2
5A03TE-25.1E	Edge	9.8	1503	35.0	7545	180.3	197.8	0.04	57.72	2.30	5.5	1.31	50.3	16.0	173.8	64.5	261.6	48.0	349.6	55.9
5A03TE-25.2C	Interior	8.4	2241	33.3	8031	105.8	145.5	0.40	39.80	4.60	9.5	2.13	85.7	26.9	273.2	99.6	385.9	71.2	519.1	80.1
5A03TE-3.1I	Interior	6.5	4479	43.9	7606	219.5	284.6	0.12	68.40	7.96	18.7	4.15	161.1	54.5	548.5	194.1	757.5	139.3	979.9	151.7
5A03TE-4.1C	Interior	10.6	2471	62.0	7137	343.8	303.8	0.05	117.85	4.45	8.7	2.45	83.8	28.7	299.0	107.4	416.6	75.6	533.3	84.7
5A03TE-4.1C	Core	12.1	9983	210.1	6775	1095.2	927.6	0.31	405.52	20.31	47.6	9.10	386.1	127.2	1285.4	450.8	1698.3	300.3	2093.7	313.2
5A03TE-6.1I	Interior	10.2	2063	55.7	7080	269.1	268.5	0.06	91.66	3.22	7.6	1.81	72.1	24.9	255.8	91.0	365.1	66.8	471.8	73.6
5A03TE-7.1C	Core	13.5	2838	65.3	8313	261.4	290.5	0.06	73.51	3.95	9.7	2.07	88.9	30.4	331.0	121.3	503.1	95.6	739.0	119.9
5A03TE-7.1E	Edge	11.1	1462	36.6	9533	170.1	222.4	0.03	43.85	1.80	4.6	0.92	40.9	14.7	171.0	61.1	259.0	50.2	378.6	59.7
5A03TE-7.2I	Interior	6.3	2727	36.2	7550	104.9	158.3	0.08	35.27	5.54	10.6	2.78	103.7	32.7	342.6	122.5	485.5	90.8	640.0	97.2
5A03TE-8.1C	Interior	11.9	2722	39.9	7055	127.6	158.2	1.13	50.49	5.94	12.6	3.14	107.6	34.0	349.9	122.6	489.2	89.2	637.6	101.1
5A03TE-8.2E	Edge	9.3	1016	26.2	9008	60.3	118.6	0.05	28.01	1.31	3.2	0.69	27.6	10.4	115.6	42.3	182.6	37.0	285.9	45.3
5A03TE-9.1E	Edge	10.1	2694	78.3	8075	620.2	520.6	0.05	119.70	4.10	9.7	2.16	88.0	31.7	331.6	115.1	466.4	84.5	595.2	95.3

[a] SHRIMP-RG spot names can be matched to grains on the CL images in Appendix A.

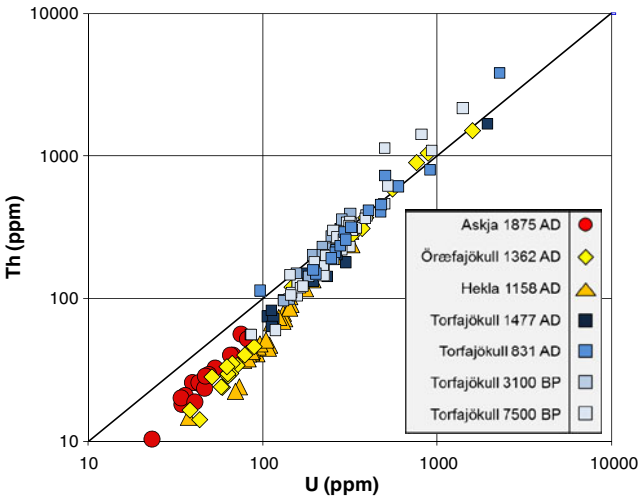

Fig. 4 Thorium (ppm) vs U (ppm) concentrations of zircon (individual SHRIMP analysis spots); log scale. Bold line represents a Th/U ratio of 1. One standard deviation for elements plotted in this paper is typically 5%

Discussion

Conditions and duration of zircon growth and storage

Elemental compositions and morphology of zircon, together with elemental compositions of host lava and pumice, provide a valuable temporal and environmental record of the silicic portions of the magmatic systems that underlie and feed these four Icelandic volcanoes. This, in turn, provides constraints on the origins of these silicic magmas. At Askja, Öræfajökull, and Hekla we have investigated zircon from single eruptions, thus providing a snapshot of the zircon entrained in erupting magmas and the records that they preserve. At Torfajökull, sampling of four eruptions that span 7000 years permits comparison of different zircon-based snapshots of the same system at different stages of its history. Below, we discuss the information provided by elemental zoning, saturation and growth temperatures, and timing of growth relative to eruption.

Elemental zoning Simple evolution of a magma, with zircon saturation and growth accompanying monotonic cooling, is expected to yield individual zircon crystals with euhedral growth zones and a core-to-rim compositional pattern of increasing Hf solid solution and decreasing Ti and Th/U (Claiborne et al. 2006, 2010b; Barth and Wooden 2010; Fohey-Breting et al. 2010). Grain-to-grain consistency with these morphological and compositional trends is expected in a zircon population extracted from a sample with a simple history. Deviations from these patterns—e.g. rounded, embayed, truncated zones; "reverse" or fluctuating compositional zoning in individual grains; ill-defined compositional patterns for the zircon population of a sample—indicate fluctuating conditions and open-system processes, potentially including extraction of zircon from ancient rocks (inheritance) or remobilization of partially solidified magma (antecrystic origin; e.g. Bacon and Lowenstern 2005; Charlier et al. 2005; Claiborne et al. 2006, 2010a,b; Miller et al. 2007; Bryan et al. 2008).

The relatively simple morphology (internal and external) of zircon crystals in this study is consistent with relatively simple magmatic histories. Exceptions and differences from sample to sample reveal some complexity, however. The well-defined contrast between dark cores and bright rims in some Öræfajökull and Torfajökull zircon crystals suggests sharp changes in conditions of growth, and the rounded zones and grain boundaries that are relatively common in the two historically erupted Torfajökull samples implies resorption events.

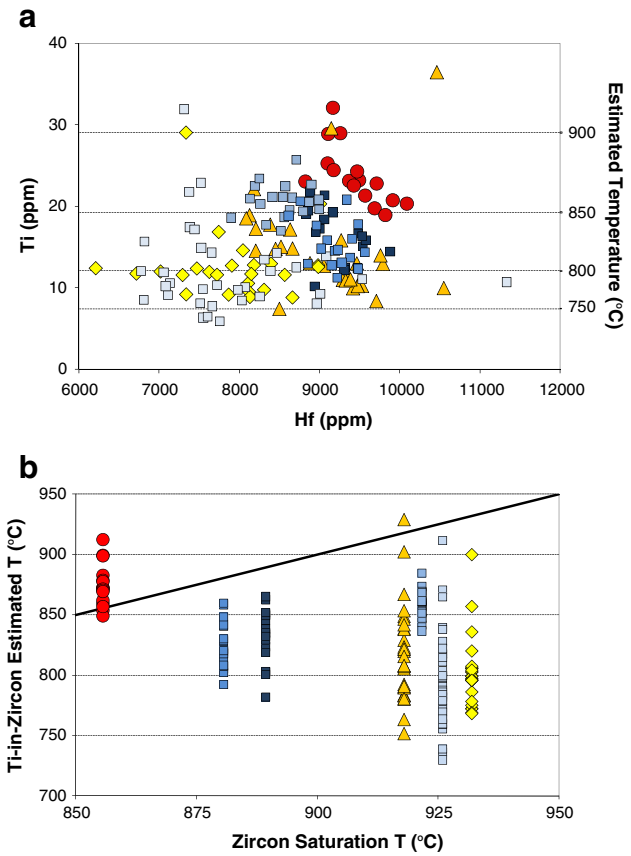

Fig. 5 **a**: Titanium vs Hf concentrations of spots analyzed by SHRIMP. Hf concentration reflects zircon fractionation (Claiborne et al. 2006) and Ti reflects temperature (Watson and Harrison, 2005; Watson et al. 2006; Ferry and Watson 2007). Temperature estimates are shown on the secondary y-axis (Ferry and Watson, 2007). Symbols as in Fig. 4. **b**: Comparing estimated Ti-in-zircon growth temperatures (Ferry and Watson 2007) to saturation temperatures for zircon from each eruption. The solid line with a slope of 1 indicates conditions in which zircon growth temperatures equal zircon saturation temperatures. Points falling above the line represent zircon growth above saturation temperatures and points falling below represent zircon growth at temperatures below the saturation temperature. Symbols as in Fig. 4

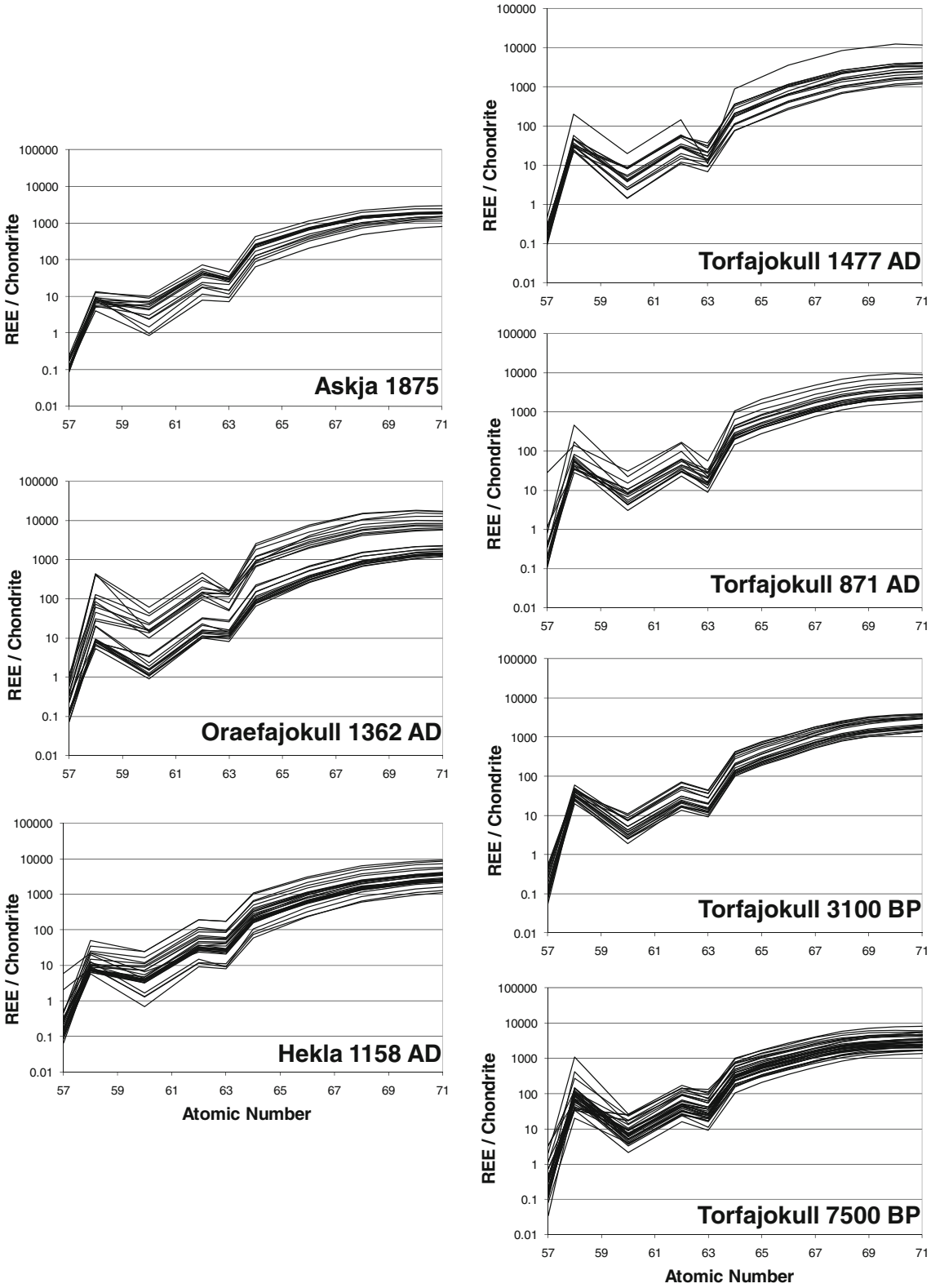

Fig. 6 Chondrite-normalized REE patterns of spots analyzed by SHRIMP (log scale)

In general, elemental trends for zircon populations from individual samples are coherent and match predictions (e.g. negative correlation of Ti and Hf concentrations), though there are well-defined contrasts from sample to sample. Although the four Torfajökull samples as a group are very broadly coherent, the group has a wide compositional

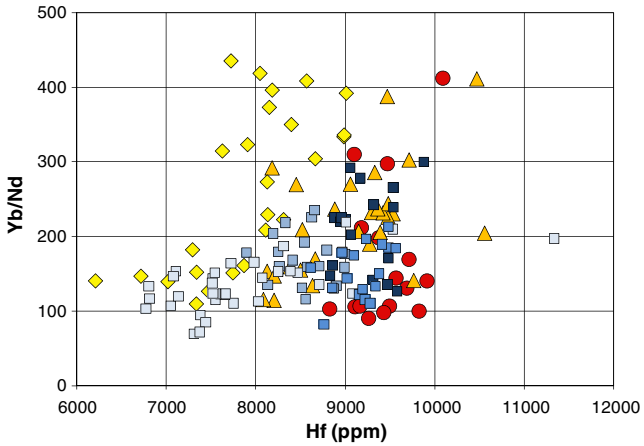

Fig. 7 HREE/LREE ratios of spots analyzed by SHRIMP (represented by Yb/Nd) vs Hf (proxy for increasing fractionation). Symbols as in Fig. 4

spread; in particular, zircon grains in the oldest eruption sample (7500 BP) are very distinct from those in the three younger samples. The zircon grains from the three younger eruptions cluster tightly, whereas zircon in the 7500 BP lava have lower Hf and a wider range of Ti and Th/U.

Compositional variability within individual grains belies the generally simple history suggested by morphology of crystals and zoning. Because of the small size of zircon crystals and the even smaller size of their internal zones, we attempted both interior and edge elemental analyses of a relatively small number of grains. Nonetheless, 38 analysis pairs representing all seven samples yielded inconsistent results: about half are normally zoned and about half reversed in terms of Hf and Ti concentrations, and this inconsistency applies to all volcanoes (Table 6). Contrast in concentrations within individual grains is commonly small, but in some cases it is very substantial, and the large discrepancies are both normal and reverse.

The absence of simple, systematic change in individual grains (e.g. consistent normal zoning, consistent reverse zoning) suggests that none of the eruptions examined in this study sampled zircon grown in uniformly evolving magmas that experienced pure, simple, monotonic fractionation. While simple fractional crystallization may be broadly responsible for petrogenesis of magma for particular eruptions, it was not a process operating in isolation. Rather, the inconsistent zoning trends imply diverse histories for grains in individual samples, some of them seemingly simple, others complex. This suggests that many, and possibly all, zircon crystals were entrained and carried to the surface in melts distinct from those in which they initially crystallized (cf. Claiborne et al. 2010a). Entrained zircon grains may have resided in rock or crystal mush that was disaggregated by ascending recharge magma on its way to eruption, or they may have been part of a resident magma that mixed with an injection of new, hotter magma. In either case, simple compositional signatures of evolution preserved within some individual zircon grains could be reversed by new growth. Importantly, the broadly coherent and distinct compositional patterns from individual samples, and for the suite of Torfajökull samples (at least the youngest three), suggest that each volcano's silicic plumbing system is tapping similar materials that form under similar conditions. This consistency may in part be responsible for generally simple and consistent zoning morphology (absence of drastic changes in conditions or melt chemistry limit resorption and minimize drastic changes in zircon composition). The low $\delta^{18}O$ values of host rocks and phenocrysts at Askja and Torfajökull provide evidence for incorporation and possible anatexis of altered upper crust, and future in situ $\delta^{18}O$ analysis of zircon will help to quantify the relative contributions of country rock delivering older zircon into the final low $\delta^{18}O$ magma.

Saturation and growth temperatures Estimated zircon saturation temperatures (855–930°C) and zircon growth temperatures (~730–930°C, from Ti-in-zircon thermometry) are relatively high for zircon from these volcanoes compared to most zircon from continental settings (Miller et al. 2003; Grimes et al. 2007; Harrison et al. 2007; Fu et al. 2008; Claiborne et al. 2010a,b; further discussion below), but similar to temperatures for zircon from the Yellowstone, USA hotspot (e.g. Bindeman et al. 2008). The high saturation temperatures reflect high concentrations of Zr in the melts (Table 2; Watson and Harrison 1983). Maximum estimated zircon growth temperatures are, with the exception of the Askja sample, very close to zircon saturation temperatures; minimum growth temperatures (excluding Askja) range from ~80 to almost 200°C lower than saturation temperature of the host melt. This finding broadly supports the idea that zircon crystals were grown in melts similar to the ones in which they were erupted, but precludes the interpretation that their growth was primarily from their host. Much or most of the growth of the zircon took place in a cooler environment than that represented by the erupting magma.

Askja zircon grains differ from the others in having estimated growth temperatures equal to or higher than saturation T, by up to 100°C, implying that the melt from which the zircon grew was richer in Zr than the erupting host magma. The temperature of the erupting magma itself has been roughly estimated to be 990–1090°C (Sigurdsson and Sparks 1981), higher than that of either zircon saturation or zircon growth. This suggests a complex history involving saturation and growth of zircon in a cooling magma, and subsequent entrainment in a second, compositionally distinct magma that was hot and zircon-undersaturated.

Table 6 Ti and Hf zoning in Individual Zircon Grains

Zircon grain	Ti interior (ppm)	Ti edge (ppm)	Ti zoning	Hf interior (ppm)	Hf edge (ppm)	Hf zoning	Consistent zoning?[a]
Askja							
1	23.2	20.7	Normal	9494	9909	Normal	Yes
2	29.0	25.3	Normal	9260	9101	~Unzoned	No
3	21.3	24.4	Reverse	9569	9178	Reverse	Yes
4	19.8	24.2	Reverse	9684	9371	Reverse	Yes
5	22.8	23.0	~Unzoned	9715	8827	Reverse	No
7	32.1	19.0	Normal	9167	9824	Normal	Yes
Hekla							
6	14.8	12.9	Normal	8454	9794	Normal	Yes
9	13.0	17.8	Reverse	8883	8387	Reverse	Yes
12	14.6	13.0	~Unzoned	8207	9468	Normal	No
14	7.4	36.5	Reverse	8502	10466	Normal	No
21	11.2	10.9	~Unzoned	9363	9329	~Unzoned	Unzoned
22	14.8	19.7	Reverse	8666	7889	Reverse	Yes
Öræfajökull							
3	12.0	11.6	Normal	7019	7294	Normal	Yes
4	29.1	12.8	Normal	7336	8982	Normal	Yes
5	20.3	12.8	Reverse	9008	8183	Reverse	Yes
7	12.4	12.7	~Unzoned	7471	7908	Normal	No
14	8.9	11.6	Reverse	8133	7723	Reverse	Yes
15	16.9	13.0	Normal	7744	8396	Normal	Yes
17	9.2	11.7	Reverse	7339	8150	Normal	No
19	10.6	12.0	Normal	8110	7627	Reverse	No
Torfajökull 1477 AD							
5	10.2	15.1	Reverse	8942	9541	Normal	No
6	12.4	14.4	Reverse	9472	9879	Normal	No
8	12.5	17.2	Reverse	9318	9003	Reverse	Yes
14	19.4	16.3	Normal	8858	9535	Normal	Yes
871 AD							
1	17.6	12.7	Normal	8964	9151	~Unzoned	No
2	20.6	17.8	Normal	8763	9482	Normal	Yes
3	11.2	12.3	~Unzoned	9220	9481	~Unzoned	Unzoned
4	13.7	15.8	Reverse	9379	9096	Reverse	Yes
6	18.8	13.0	Normal	8615	8854	~Unzoned	No
9	14.7	16.0	Reverse	9194	9408	Normal	No
3100 BP							
1	20.8	19.5	~Unzoned	8993	8627	Reverse	No
7500 BP							
2	5.9	10.7	Reverse	7753	11335	Normal	No
7	6.3	11.1	Reverse	7550	9533	Normal	No
8	11.9	9.3	Normal	7055	9008	Normal	Yes
15	7.7	8.1	~Unzoned	7666	8967	Normal	No
21	14.9	8.9	Normal	7525	8253	Normal	Yes
22	17.2	12.1	Normal	7442	8389	Normal	Yes
24	8.1	9.8	~Unzoned	7514	7982	Normal	No

[a] "Consistent zoning" means that both Hf and Ti display the same of zoning pattern (both normal, or both reverse).

Table 7 Summary of zircon features considered in silicic petrogenesis investigation

Eruption	Ti zoning: norm./rev./un.[a]	Hf zoning: norm./rev/un.[b]	Ti-Hf zoning consistency: (yes/no/un.)[c]	Ti-in-zircon temp. range (°C)	zircon saturation Temp. (°C)	discrete interiors	rounded interiors	rounded exteriors	range of Ages (ka)
Askja 1875 AD	3/2/1[d]	2/3/1	4/2/0	850-910	855	None	n/a	Few-to-none	Unavailable
Öræfajökull 1362 AD	4/3/1	5/3/0	5/3/0	770-900	930	Many	Many	Few-to-none	0–20, 35
Hekla 1158 AD	1/3/2	3/2/1	3/2/1	750–930	920	Few	None	Few-to-none	0–30, 45
Torfajökull 1477 AD	1/3/0	3/1/0	2/2/0	780–865	890	Some	Some	Many	0–20, 45
871 AD	3/2/1	2/1/3	2/3/1	790–860	880	Some	Some	Some	10–30
3100 BP	0/0/1	0/1/0	0/1/0	840–885	920	Some	Few-to-none	Few-to-none	15–40
7500 BP	3/2/2	7/0/0	3/4/0	730–910	925	Some	Few-to-none	Few-to-none	10–15, 35–40

[a] Normal = higher Ti in interior than at edge; "un" indicates that measured concentrations were very similar and we designated them as unzoned

[b] Normal = lower Hf in interior than at edge; "un" indicates that measured concentrations were very similar and we designated them as unzoned

[c] By "consistency" we mean that both Ti and Hf show the same type of zoning (either both normal or both reverse).

[d] We conducted multiple SHRIMP trace element analyses on 6 grains from Askja (3+2+1). The same scheme applies to the other samples.

Timing of growth relative to eruptions In the simplest case, where zircon crystals grow in host magma during storage and heat loss prior to eruption, ages of growth would span the time between saturation and eruption. Uranium-thorium model disequilibria ages for the samples investigated for this study are not consistent with such a history.

While zircon populations from each individual eruption have variable age distributions, all display evidence for extensive zircon growth that predates eruptions by more than 10 k.y.: in fact, more than 70% of the ages for all samples except Öræfajökull are older than 10 ka. Model ages range upward to 50 ka, with a majority (almost 60%) falling in the range 10–30 ka. With the exception of Torfajökull 871 and 7500 AD, each sample also has several ages that are younger than 10 ka (Öræfajökull is distinguished by having a majority of sub-10 ka ages). The predominance of older ages and the relatively small number of sub-10 ka ages suggests that the zircon crystals grew and were stored in a zone with a history separate from that of the erupting magma. This lengthy history contrasts with that of major phases in the 1477 and 871 AD eruptions of Torfajokull, for which Zellmer et al. (2008) report pre-eruptive crystallization at 0–3 ka, suggesting that crystal inheritance played a minor role. Similar contrasts between major phase and zircon history has been reported for other systems, e.g. at Tarawera, New Zealand and Mount St. Helens and South Sister, USA (Klemetti and Cooper 2007; Claiborne et al. 2010a; Stelten and Cooper 2010), where zircon is interpreted to be derived from long-lived storage zones and major phase ages better reflect the ascending and erupting magma.

Although the relatively long interval between most of the zircon growth and eruption is critical for relating the history of zircon growth relative to that of the host magma, it is also noteworthy that this interval of <50 k.y. is short compared to that which has recently been demonstrated for many other volcanoes through in situ dating of zircon (e.g. survey by Simon et al. 2008; Long Valley, USA, Reid et al. 1997; Taupo Zone, New Zealand, Brown and Fletcher 1999; Charlier et al. 2003, 2005; Yellowstone, USA, Bindeman et al. 2001; Vazquez and Reid 2002; Crater Lake, USA, Bacon and Lowenstern 2005; Mount St. Helens, USA, Claiborne et al. 2010a).

Implications of the zircon record in young Icelandic volcanoes Morphology, zoning patterns, compositions, and U-Th ages of zircon from the samples we have studied from Askja, Hekla, Torfajökull, and Öræfajökull (summarized in Table 7) all point to growth and storage in a subvolcanic silicic mush or recently solidified rock, at temperatures above the solidus but lower than that of the erupting magma. The products we sampled were likely ascending magmas that entrained a zircon cargo that formed up to tens of thousands of years preceding the eruptive event. The older zircon grains in low- $\delta^{18}O$ Torfajökull pumice may be inherited from older, solid, hydrothermally-altered rocks reflecting processes similar to those advocated for zircon origins at Yellowstone (e.g. Bindeman et al. 2001; zircon from the low- $\delta^{18}O$ Askja pumice may have similar origins, but we have not obtained ages that might test that hypothesis).

Relation between zircon compositions and tectonic setting

Distinctive compositional characteristics of zircon from our samples may reflect the tectonic environments in which their host magmas formed. Most obviously, Ti vs Hf trends for the volcanoes are distinct and can plausibly be correlated to tectonic setting.

The monotonically decreasing Ti vs. Hf trends are aligned in such a way that, for a given Hf value, Askja (on-rift) has the highest Ti (and implied temperatures), followed by Torfajökull (on rift, near termination), followed

by Hekla (transitional to rift), followed (mostly) by Öræfajökull, with the lowest Ti at a given Hf concentration (off-rift; Fig. 8). To put it another way, for the same degree of fractionation as indicated by Hf, zircon crystals growing in magmatic systems nearest the rift grow at higher temperatures. For a given Ti concentration, Askja (on rift) has the highest Hf, followed by Torfajökull 3100 BP-1477 AD (on rift, near termination), followed by Hekla (transitional to rift), followed (mostly) by Öræfajökull (off-rift).

The Ti vs. Hf (~temperature vs. fractionation) data for Torfajökull 7500 BP and Öræfajökull zircon do not define sub-parallel, linear, patterns that are evident for the other eruptions that were sampled. Both of these samples have fairly wide ranges of Hf, but Hf is generally lower than those for the other eruptions, and Ti (~temperatures) is lower at a given Hf concentration. The thermal-fractionation history recorded by these zircon grains suggests that the off-rift Öræfajökull zircon and the transitional-to-rift 7500 BP Torfajökull zircon were growing in magmas that experienced a different sort of petrogenetic history than magmas at on-rift Hekla, younger Torfajökull and Askja.

Iceland zircon in a global context

Figure 9a, b and c compare the compositions of Icelandic zircon, as represented by our initial data set, with zircon globally (our compilation of analyses from Vanderbilt-Stanford/USGS SHRIMP collaborations representing a wide range of tectonic settings; compilation of Grimes et al. 2007).

The Icelandic zircon compositions plot in a relatively restricted field on these diagrams that most closely matches that of Alid, a rift-related volcano in Eritrea near the Red Sea (Lowenstern et al. 1997, 2006). They are distinguished by their low and restricted Hf, Th/U higher than those at Mount St. Helens (arc volcano) and lower than those extension-related granites and rhyolites in mature continental crust (Nevada-Arizona, USA). They lie near, but above, the boundary on a U/Yb vs. Hf plot that Grimes et al. (2007) propose distinguishes MORB from continental zircon (on the high-U/Yb, continental side).

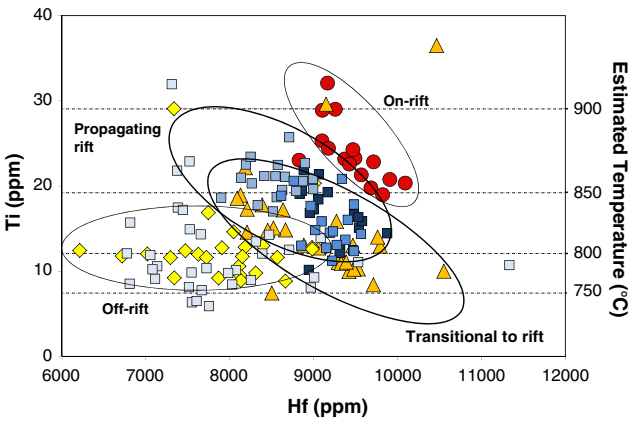

Fig. 8 Titanium vs Hf concentrations of SHRIMP spot analyses with context of tectonic setting. Ellipses are drawn around the dominant clusters of data points for each volcano (excluding outliers): Askja, on-rift; Torfajökull, propagating rift-tip; Hekla, transitional to rift; Öræfajökull, off-rift. Note that the majority of Ti and Hf analyses for the oldest eruption of Torfajökull , 7500 BP, fall within the ellipse drawn for off-rift Öræfajökull. Individual data point symbols are as in Fig. 4

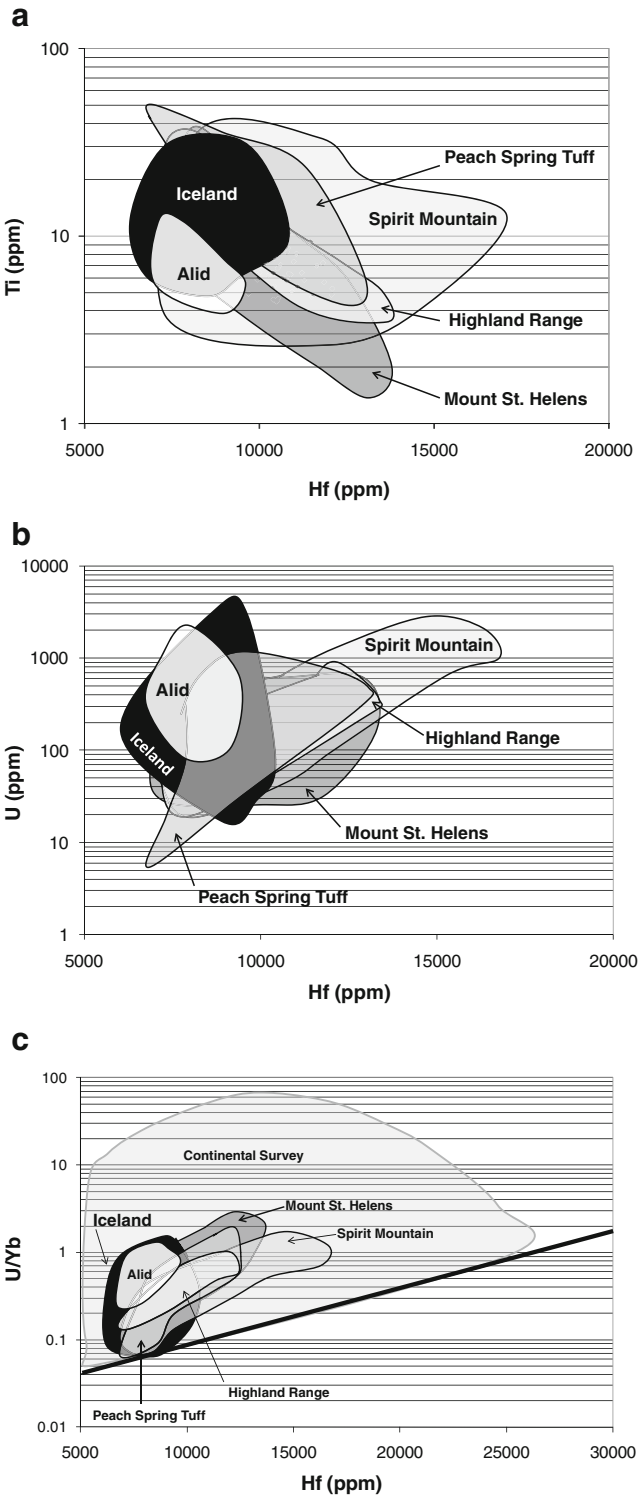

◀ **Fig. 9** **a**: Comparison of Ti vs Hf for Icelandic zircon and zircon from an active continental rift generating new oceanic lithosphere (Alid volcano, Eritrea [granophyre enclave, rhyolite; Lowenstern et al. 1997, 2006; Flanagan et al. 2010]); onset of continental extension (Colorado River Extensional Corridor, USA: Highland Range [rhyolite; Colombini et al. 2011], Spirit Mountain batholith [granite-quartz monzonite; Claiborne et al. 2006, 2010a], Peach Spring Tuff [rhyolite-trachyte; Pamukcu 2010]); subduction-related continental arc volcano (Mount St. Helens [dacite; Claiborne et al. 2010b]). **b**: U vs Hf concentrations, same populations as in (**a**). **c**: U/Yb vs Hf concentrations. Comparison between zircon populations of (**a**) with distinction between continental- and MORB-type zircon proposed by Grimes et al. (2007). The "Continental Survey" field is also from Grimes et al. (2007) and was based on >1500 SHRIMP-RG analyses of continental zircon

Based upon Hf and Y concentrations alone, Pupin (2000) distinguished zircon from granitoid suites of different types and environments. In particular, he noted that Hf concentrations are low (<10000 ppm) and Y concentrations range widely and reach high values (>4000 ppm) in plagiogranites and other granitoids associated directly with juvenile mafic magmas. Granitoids associated with thickened orogenic crust, in contrast, have opposite Hf-Y relationships (low and restricted Y, wide range of Hf up to much higher concentrations). Our data for Iceland and the compilations presented here are consistent with these generalizations (Fig. 9a,b,c; Table 5).

Conclusions

This study is the first to use zircon as a lens for examining the petrogenesis of silicic magmas in Iceland. Zircon grains from recent (primarily historical) eruptions are small and sparse, but they record important information about the magmas in which they grew. Uranium-thorium dating reveals growth ages predating eruption by up to 50 ka, with most ages falling in a range of 5–30 ka, a time sufficiently long to permit long crystallization histories or recycling from a crystal mush or a hydrothermally altered rock (e.g. Bacon and Lowenstern 2005; Bindeman et al. 2008; Claiborne et al. 2010a). Recognition of these different petrogenetic processes is best achieved by the additional isotope fingerprinting of zircon that we plan in the future. Although most zircon growth substantially predated eruption, the range of ages is far less than has been found in arc and continental interior settings, where zircon ages commonly predate the time of eruption by hundreds of thousands of years (e.g. Brown and Fletcher 1999, Bindeman et al. 2001; Vazquez and Reid 2002; Claiborne et al. 2010a). The zircon have Ti concentrations that range from ~10–30 ppm (corresponding to estimated growth temperatures of ~750–900°C), which is relatively high compared to most of those reported from either intrusive or extrusive rocks (e.g. Discussion, this study; Claiborne et al. 2006, 2010a,b; Harrison et al. 2007; Fu et al. 2008). Ti concentrations and calculated temperatures correlate with expected thermal conditions for the local tectonic settings of the individual Icelandic volcanic centers. For a given Hf concentration (representative of degree of fractionation) the Askja (on-rift, near hotspot) zircon grains have the highest measured Ti and estimated temperature followed by Torfajökull (on rift, near termination), Hekla (transitional to rift) and Öræfajökull (off-axis).

Multiple lines of evidence, including U-Th ages that substantially predate eruptions and the absence of consistent normal zoning, suggest that the grains did not grow from magma that experienced simple, monotonic fractionation. While simple fractional crystallization may be broadly responsible for petrogenesis of the silicic magmas, zircon ages and compositional patterns, together with the low $\delta^{18}O$ values of some of the studied units, demonstrate that it was not a process operating in isolation. The results of this study indicate that zircon was liberated from disaggregated, partially melted rock, crystal mush, and ponded magma and then entrained in hot, silicic magma replenishments that transported them to eruption.

Acknowledgments We give special thanks to Kenneth Brown, Christina Carter and Nicole Fohey-Breting for their pioneering work with prehistoric Torfajökull zircon, made possible by the IUPUI Undergraduate Research Opportunity Program. We also thank Olgeir Sigmarsson, Gudrun Larsen, Karl Gronvold, Peter Oswald, Denny Geist, Karen Harpp, Ken Rubin, Georg Zellmer, and Sheila Seaman for invaluable advice concerning the meaning of silicic magmatism in Iceland and practicalities of investigating it in the field. Jorge Vasquez and Frank Mazdab provided assistance at the Stanford-USGS SHRIMP lab, and Abraham Padilla, Addy Petrilla, Lily Claiborne, and Danny Flanagan worked with us in the field and lab. This research was supported by a Geological Society of America Student Research Grant and National Science Foundation Grant NSF- NSF-EAR-0635922.

References

Arnorsson S, Ivarsson G, Cuff KE, Saemundsson K (1987) Geothermal activity in the Torfajokull Field, south Iceland; summary of geochemical studies. Jökull 37:1–12

Bacon CR, Lowenstern JB (2005) Late Pleistocene granodiorite source for recycled zircon and phenocrysts in rhyodacite lava at Crater Lake, Oregon. Earth Planet Sci Lett 233:277–293. doi:10.1016/j.epsl.2005.02.012

Barth AP, Wooden JL (2010) Coupled elemental and isotopic analyses of polygenetic zircons from granitic rocks by ion microprobe, with implications for melt evolution and the sources of granitic magmas. Chem Geol 277:149–159

Bea F (1996) Residence of REE, Y, Th and U in granites and crustal protoliths; Implications for the chemistry of crustal melts. J Petrol 37:521–552

Bindeman I (2008) Oxygen isotopes in mantle and crustal magmas as revealed by single crystal analysis. Rev Mineral Geochem 69:445–478. doi:10.2138/rmg.2008.69.12

Bindeman IN, Valley JW, Wooden JL, Persing HM (2001) Post-caldera volcanism: in situ measurement of U-Pb age and oxygen isotope ratio in Pleistocene zircons from Yellowstone caldera. Earth Planet Sci Lett 189:197–206

Bindeman IN, Fu B, Kita N, Valley JW (2008) Origin and evolution of Yellowstone silicic magmatism based on ion microprobe analysis of izotopically-zoned zircons. J Petrol 49:163–193

Blake S (1984) Magma mixing and hybridization processes at the alkalic, silicic, Torfajoekull central volcano triggered by tholeiitic Veidivoetn fissuring, South Iceland. J Volcanol Geotherm Res 22:1–31

Brown SJA, Fletcher IR (1999) SHRIMP U-Pb dating of the preeruption growth history of zircons from the 340 ka Whakamaru Ignimbrite, New Zealand: Evidence for >250 k.y. magma residence times. Geology 27:1035–1038. doi:10.1130/0091-7613(1999)027<1035:supdot>2.3.co;2

Brown KL, Carter CA, Fohey NK, Wooden JL, Yi K, Barth AP (2004) A study of the origin of rhyolite at mid-ocean ridges; geochronology and petrology of trachydacite and rhyolite from Salton Sea, California, and Torfajokull, Iceland. Abstracts with Programs—Geol Soc Am 36: 79

Bryan SE, Ferrari L, Reiners PW, Allen CM, Petrone CM, Ramos-Rosique A, Campbell IH (2008) New insights into crustal contributions to large-volume rhyolite generation in the mid-Tertiary Sierra Madre Occidental province, Mexico, revealed by U-Pb geochronology. J Petrol 49:47–77

Carmichael ISE (1964) The petrology of Thingmuli, a Tertiary volcano in eastern Iceland. J Petrol 5:435–460

Carmichael ISE, Turner FJ, Verhoogen J (1974) Igneous petrology. McGraw-Hill Book Co., New York

Charlier BLA, Peate DW, Wilson CJN, Lowenstern JB, Storey M, Brown SJA (2003) Crystallisation ages in coeval silicic magma bodies: ^{238}U-^{230}Th disequilibrium evidence from the Rotoiti and Earthquake Flat eruption deposits. Taupo Volcanic Zone, New Zealand. Earth Planet Sci Lett 206:441–457

Charlier BLA, Wilson CJN, Lowenstern JB, Blake S, Van Calsteren PW, Davidson JP (2005) Magma generation at a large, hyperactive silicic volcano (Taupo, New Zealand) revealed by U-Th and U-Pb systematics in zircons. J Petrol 46:3–32. doi:10.1093/petrology/egh060

Claiborne LL, Miller CF, Walker BA, Wooden JL, Mazdab FK, Bea F (2006) Tracking magmatic processes through Zr/Hf ratios in rocks and Hf and Ti zoning in zircons: an example from the Spirit Mountain batholith, Nevada. Mineral Mag 70:517–543. doi:10.1180/0026461067050348

Claiborne LL, Miller CF, Flanagan DM, Clynne MA, Wooden JL (2010a) Zircon reveals protracted magma storage and recycling beneath Mount St. Helens. Geology 38:1011–1014. doi:10.1130/g31285.1

Claiborne LL, Miller CF, Wooden JL (2010b) Trace element composition of igneous zircon: a thermal and compositional record of the accumulation and evolution of a large silicic batholith. Spirit Mountain, Nevada. Contrib Mineral Petrol 160:511–531. doi:10.1007/s00410-010-0491-5

Colombini L, Miller CF, Gualda GAR, Wooden JL, Miller JS (2011) Sphene (titanite) and zircon in the Highland Range volcanic sequence (Miocene, Southern Nevada, USA): Elemental partitioning, phase relations, and influence on evolution of silicic magma. Mineral Petrol, this issue.

Condomines M, Morand P, Allegre CJ, Sigvaldason G (1981) Th-230-U-238 Disequilibria in Historical Lavas from Iceland. Earth Planet Sci Lett 55:393–406

Crowley JL, Schoene B, Bowring SA (2007) U-Pb dating of zircon in the Bishop Tuff at the millennial scale. Geology 35:1123–1126. doi:10.1130/G24017A.1

Ferry JM, Watson EB (2007) New thermodynamic models and revised calibrations for the Ti-in-zircon and Zr-in-rutile thermometers. Contrib Mineral Petrol 154:429–437. doi:10.1007/s00410-007-0201-0

Flanagan DM, Lowenstern JB, Carley TL, Miller CF, Wooden JL (2010) Zircon from the Alid volcanic center, Eritrea: implications for magmatic evolution. Abstracts with Programs—Geol Soc Am 42:668.

Fohey-Breting NK, Barth AP, Wooden JL, Mazdab FK, Carter CA, Schermer ER (2010) Relationship of voluminous ignimbrites to continental arc plutons: petrology of Jurassic ignimbrites and contemporaneous plutons in southern California. J Volcano Geotherm Res 189:1–11

Fu B, Page FZ, Cavosie AJ, Fournelle J, Kita NT, Lackey JS, Wilde SA, Valley JW (2008) Ti-in-zircon thermometry: applications and limitations. Contrib Mineral Petrol 156:197–215. doi:10.1007/s00410-008-0281-5

Grimes CB, John BE, Kelermen PB, Mazdab FK, Wooden JL, Cheadle MJ, Hanghoj K, Schwartz JJ (2007) Trace element chemistry of zircons from oceanic crust: a method for distinguishing detrital zircon provenance. Geology 35:643–646. doi:10.1130/G23603a.1

Gronvold K, Larsen G, Einarsson P, Thorarinsson S, Saemundsson K (1983) The Hekla eruption 1980–1981. Bull Volcano 46:349–363

Gunnarsson B, Marsh BD, Taylor HP (1998) Generation of Icelandic rhyolites: silicic lavas from the Torfajokull central volcano. J Volcano Geotherm Res 83:1–45

Harrison TM, Watson EB, Aikman AB (2007) Temperature spectra of zircon crystallization in plutonic rocks. Geology 35:635–638. doi:10.1130/g23505a.1

Hayden LA, Watson EB (2007) Rutile saturation in hydrous siliceous melts and its bearing on Ti-thermometry of quartz and zircon. Earth Planet Sci Lett 258:561–568

Hoskin PWO, Schaltegger U (2003) The composition of zircon and igneous and metamorphic petrogenesis. Rev Mineral Geochem 53:27–62. doi:10.2113/0530027

Jonasson K (2007) Silicic volcanism in Iceland: composition and distribution within the active volcanic zones. J Geodyn 43:101–117. doi:10.1016/j.jog.2006.09.004

Klemetti E, Cooper K (2007) Cryptic young zircon and young plagioclase in the Kaharoa Rhyolite, Tarawera, New Zealand: Implications for crystal recycling in magmatic systems. Eos, Trans, Am Geophys Un Abstract #V42C-05.

Lacasse C, Sigurdsson H, Carey SN, Johannesson H, Thomas LE, Rogers NW (2003) Bimodal volcanism at the Katla subglacial caldera. Iceland: insight into the geochemistry and petrogenesis of rhyolitic magmas. Bull Volcano 69:373–399

Larsen G, Dugmore A, Newton A (1999) Geochemistry of historical-age silicic tephras in Iceland. Holocene 9:463–471

Lowenstern JB, Clynne MA, Bullen TD (1997) Comagmatic A-type granophyre and rhyolite from the Alid volcanic center, Eritrea, northeast Africa. J Petrol 38:1707–1721

Lowenstern JB, Persing HM, Wooden JL, Lanphere M, Donnelly-Nolan J, Grove TL (2000) U-Th dating of single zircons from young granitoid xenoliths: new tools for understanding volcanic processes. Earth Planet Sci Lett 183:291–302

Lowenstern JB, Charlier BLA, Clynne MA, Wooden JL (2006) Extreme U-Th disequilibrium in rift-related basalts, rhyolites and granophyric granite and the timescale of rhyolite generation, intrusion and crystallization at Alid volcanic center, Eritrea. J Petrol 47:2105–2122. doi:10.1093/petrology/egl038

Macdonald R, Sparks RSJ, Sigurdsson H, Mattey DP, Mcgarvie DW, Smith RL (1987) The 1875 eruption of Askja volcano, Iceland—combined fractional crystallization and selective contamination in the generation of rhyolitic magma. Mineral Mag 51:183–202

Macdonald R, Mcgarvie DW, Pinkerton H, Smith RL, Palacz ZA (1990) Petrogenetic evolution of the Torfajokull Volcanic Complex, Iceland.1. Relationship between the magma types. J Petrol 31:429–459

Martin E, Sigmarsson O (2007) Crustal thermal state and origin of silicic magma in Iceland: the case of Torfajokull, Ljosufjoll and Snaefellsjokull volcanoes. Contrib Mineral Petrol 153:593–605. doi:10.1007/s00410-006-0165-5

Martin E, Sigmarsson O (2010) Thirteen million years of silicic magma production in Iceland: links between petrogenesis and tectonic settings. Lithos 116:129–144

Miller CF, McDowell SM, Mapes RW (2003) Hot and cold granites? Implications of zircon saturation temperatures and preservation of inheritance. Geology 31:529–532. doi:10.1130/0091-7613(2003)031<0529:hacgio>2.0.co;2

Miller JS, Matzel JEP, Miller CF, Burgess SD, Miller RB (2007) Zircon growth and recycling during the assembly of large, composite arc plutons. J Volcano Geothermal Res 167:282–299

Mork ME (1984) Magma mixing in the post-glacial veidivotn fissure eruption, southeast Iceland—a microprobe study of mineral and glass variations. Lithos 17:55–75

Muehlenbachs K, Anderson AT Jr, Sigvaldason GE (1974) Low-O18 basalts from Iceland. Geochim Cosmochim Acta 38:577–588

O'Hara MJ, Fry N, Prichard HM (2001) Minor phases as carriers of trace elements in non-modal crystal-liquid separation processes; II, Illustrations and bearing on behaviour of REE, U, Th and the PGE in igneous processes. J Petrol 42:1887–1910

Oswald P, Geist D, Harpp K, Christensen B, Wallace P, Anonymous (2007) Differentiation of historical Hekla magmas. Eos, Trans, Am Geophys Un Abstract #V13C-1493.

Pamukcu A (2010) The evolution of the Peach Spring Tuff magmatic system as revealed by accessory mineral textures and compositions, MSc thesis: Vanderbilt University, Nashville, TN.

Prestvik T, Goldberg S, Karlsson H, Gronvold K (2001) Anomalous strontium and lead isotope signatures in the off-rift Oraefajokull central volcano in south-east Iceland. Evidence for enriched endmember(s) of the Iceland mantle plume? Earth Planet Sci Lett 190:211–220

Pupin J (2000) Granite genesis related to geodynamics from Hf-Y in Zircon. Trans Royal Soc Edinb Earth Sci 91:245–256

Reid MR, Coath CD, Harrison TM, McKeegan KD (1997) Prolonged residence times for the youngest rhyolites associated with Long Valley Caldera; ^{230}Th - ^{238}U ion microprobe dating of young zircons. Earth Planet Sci Lett 150:27–39

Rose-Koga EF, Sigmarsson O (2008) B-O-Th isotope systematics in Icelandic tephra. Chem Geol 255:454–462

Saemundsson K (1979) Outline of the geology of Iceland. Jökull 29:7–28

Sawka WN, Chappell BW (1988) Fractionation of uranium, thorium and rare-earth elements in a vertically zoned granodiorite—implications for heat-production distributions in the Sierra-Nevada Batholith, California, USA. Geochimica Et Cosmochimica Acta 52(5):1131–1143

Schmitt AK, Stockli DF, Lindsay JM, Robertson R, Lovera OM, Kislitsyn R (2010) Episodic growth and homogenization of plutonic roots in arc volcanoes from combined U–Th and (U–Th)/He zircon dating. Earth Planet Sci Lett 295:91–103. doi:10.1016/j.epsl.2010.03.028

Selbekk RS, Tronnes RG (2007) The 1362 AD Oraefajoull eruption, Iceland: petrology and geochemistry of large-volume homogeneous rhyolite. J Volcano Geothermal Res 160:42–58. doi:10.1016/j.jvolgeores.2006.08.005

Sharma K, Self S, Blake S, Thordarson T, Larsen G (2008) The AD 1362 Oraefajokull eruption, S.E. Iceland; physical volcanology and volatile release. J Volcano Geothermal Res 178:719–739

Sigurdsson H, Sparks RSJ (1981) Petrology of rhyolitic and mixed magma Ejecta from the 1875 eruption of Askja, Iceland. J Petrol 22:41–84

Sigvaldason GE (2002) Volcanic and tectonic processes coinciding with glaciation and crustal rebound: an early Holocene rhyolitic eruption in the Dyngjufjoll volcanic centre and the formation of the Askja caldera, north Iceland. Bull Volcano 64:192–205. doi:10.1007/s00445-002-0204-7

Simon JI, Renne PR, Mundil R (2008) Implications of pre-eruptive magmatic histories of zircons for U-Pb geochronology of silicic extrusions. Earth Planet Sci Lett 266:182–194

Sparks RSJ, Wilson L, Sigurdsson H (1981) The pyroclastic deposits of the 1875 eruption of Askja, Iceland. Phil Trans Royal Soc London Series A-Math Phys Eng Sci 299:241–273

Stelten M, Cooper KM (2010) Constraints on the nature of the subvolcanic system at South Sister Volcano, Oregon from ^{238}U-^{230}Th zircon ages and ^{238}U-^{230}Th-^{226}Ra plagioclase ages. Abstracts with Programs - Geological Society of America 42: 668.

Sverrisdottir G (2007) Hybrid magma generation preceding Plinian silicic eruptions at Hekla, Iceland: evidence from mineralogy and chemistry of two zoned deposits. Geol Mag 144:643–659. doi:10.1017/S0016756807003470

Thorarinsson S (1958) The Oraefajokull eruption of 1362. Acta Naturalia Islandica 2,Natturugripasafn Islands Museum Rerum Naturalium Islandiae, Reykjavik.

Thordarson T, Hoskuldsson A (2002) Iceland. Classic Geology in Europe 3, Terra Publishing, Harpenden, England.

Thordarson T, Larsen G (2007) Volcanism in Iceland in historical time: volcano types, eruption styles and eruptive history. J Geodyn 43:118–152. doi:10.1016/j.jog.2006.09.005

Vazquez JA, Reid MR (2002) Time scales of magma storage and differentiation of voluminous high-silica rhyolites at Yellowstone Caldera, Wyoming. Contrib Mineral Petrol 144:274–285

Walker GPL (1966) Acid volcanic rocks in Iceland. Bull Volcano 29:375–402

Watson EB, Harrison TM (1983) Zircon saturation revisited—temperature and composition effects in a variety of crustal magma types. Earth Planet Sci Lett 64:295–304

Watson EB, Harrison TM (2005) Zircon thermometer reveals minimum melting conditions on earliest Earth. Science 308:841–844. doi:10.1126/science.1110873

Watson EB, Wark DA, Thomas JB (2006) Crystallization thermometers for zircon and rutile. Contrib Mineral Petrol 151:413–433. doi:10.1007/s00410-006-0068-5

Wood DA (1978) Major and trace element variations in the Tertiary lavas of eastern Iceland and their significance with respect to the Iceland geochemical anomaly. J Petrol 19:393–436

Wood DA, Joron JL, Treuil M, Norry M, Tarney J (1979) Elemental and Sr isotope variations in basic lavas from Iceland and the surrounding ocean floor; the nature of mantle source inhomogeneities. Contrib Mineral Petrol 70:319–339

Zellmer GF, Rubin KH, Gronvold K, Jurado-Chichay Z, Hernandez-Trevino T (2004) U-series whole-rock and mineral geochemistry of recent bimodal eruptive products from the Torfajokull/Veidivotn volcanic system, south-central Iceland. Eos, Trans, Am Geophys Un Abstract #V53A-0602.

Zellmer GF, Rubin KH, Gronvold K, Jurado-Chichay Z (2008) On the recent bimodal magmatic processes and their rates in the Torfajokull-Veidivotn area, Iceland. Earth Planet Sci Lett 269:387–397. doi:10.1016/j.epsl.2008.02.026